Original paper

Multistage hydrothermal vein mineralization in low-grade metamorphosed rocks: Chříč locality, Teplá-Barrandian Unit, Bohemian Massif, Czech Republic

Karel ŽÁK[1]*, Lukáš ACKERMAN[1], František VESELOVSKÝ[2], Jan PAŠAVA[2], Petr DOBEŠ[2], Martin SVOJTKA[1], Robert A. CREASER[3]

[1] *Institute of Geology of the Czech Academy of Sciences, Rozvojová 269, 165 00 Praha 6, Czech Republic; zak@gli.cas.cz; svojtka@gli.cas.cz; ackerman@gli.cas.cz*

[2] *Czech Geological Survey, Geologická 6, 152 00 Praha 5, Czech Republic; frantisek.veselovsky@geology.cz; jan.pasava@geology.cz; petr.dobes@geology.cz*

[3] *University of Alberta, 3-18A Earth Sciences Building, 11223 Saskatchewan Drive NW, Edmonton AB T6G 2E3, Canada; robert.creaser@ualberta.ca*

* *Corresponding author; current address: karel.zak.geo@gmail.com*

A small and isolated hydrothermal vein-type Sb deposit is hosted by a lamprophyre dike which penetrated Neoproterozoic to early Cambrian volcanosedimentary successions near Chříč in the Teplá–Barrandian Unit, Czech Republic. Hydrothermal minerals were formed in several consecutive mineralization stages, separated by long pauses in hydrothermal fluid flow. Early Stage I is characterized by the formation of carbonates of dolomite-ankerite series (Carb I) and arsenopyrite with an imprecise Re–Os age of ~570 to 510 Ma. Stage I was followed by tectonic movements and brecciation. The second mineralization stage (Stage II) is characterized by the precipitation of quartz (Qtz I) and Sb minerals (predominantly stibnite) while the third stage (Stage III) is marked by the presence of carbonates of dolomite-ankerite series (Carb II) and quartz (Qtz II) along with Cu, Zn, Pb, Ag and Fe sulfides. Lead isotope data of galena indicate a Variscan age of Stages II–III. These stages were followed by precipitation of another generation of carbonate of dolomite–ankerite series (Carb III, Stage IV), quartz (Qtz III, Stage V) and formation of Sb supergene minerals. The earlier reported occurrence of gold was not confirmed in the studied rock samples but three types of gold particles of variable fineness, with one of them indicating a local origin, were found in the heavy mineral concentrate from a local creek. Elevated Au concentrations were found in arsenopyrite and pyrite. The ore-forming hydrothermal fluid of the mineralization stage III was of H_2O–CO_2 type with minor CH_4 admixture, medium salinity, and temperatures in the range of 258–350 °C with an observed temperature decrease from Stage II to Stage V. Oxygen isotope data of Carb II correspond to high $\delta^{18}O_{fluid}$ values (~ +7.5 ‰ VSMOW) with a decrease in the fluid $\delta^{18}O$ to later stages. An important part of the carbonate carbon was derived from decomposition of organic matter or its high-temperature reaction with hydrothermal fluid. Considering the wide variation in $\delta^{34}S$ values of sulfides and elevated Sb contents in the TBU black shales, we anticipate that the origin of the Chříč mineralization is closely associated with a metal and carbon-sulfur remobilization from the TBU volcanosedimentary successions in response to Cadomian and Variscan tectonothermal events.

Keywords: Teplá–Barrandian Unit, Cadomian and Variscan hydrothermal mineralization, Sb ore, fluid inclusions, sulfur, carbon oxygen and lead isotopes, Re-Os arsenopyrite dating, ore genesis

Received: 20 March 2023; accepted: 17 October 2023; handling editor: M. Števka

The online version of this article (doi: 10.3190/jgeosci.381) contains supplementary electronic material (ESM).

1. Introduction

The Bohemian Massif hosts many types of hydrothermal vein-type ore mineralization with various metal associations (Bernard 1991; Bernard and Žák 1992; Žák et al. 1996; Němec and Zachariáš 2018). Many of these ore systems usually occur in high- to medium-grade metamorphosed units in a spatial relationship to Variscan granitoids, or in low-grade metamorphosed units along crustal block boundaries (cf. Beaudoin et al. 1999; Němec and Zachariáš 2018). Therefore, their formation is generally assumed to be genetically related to Variscan (~370–310 Ma) tectono-magmatic and metamorphic events, or to post-Variscan extensional tectonic events. However, metals as well as sulfur and carbon seem to be derived from multiple sources, including the Neoproterozoic–Cambrian volcanosedimentary successions of the Teplá–Barrandian Unit (TBU) of the studied area (e.g., Morávek and Pouba 1987; Žák and Dobeš 1991). In contrast, hydrothermal vein-type min-

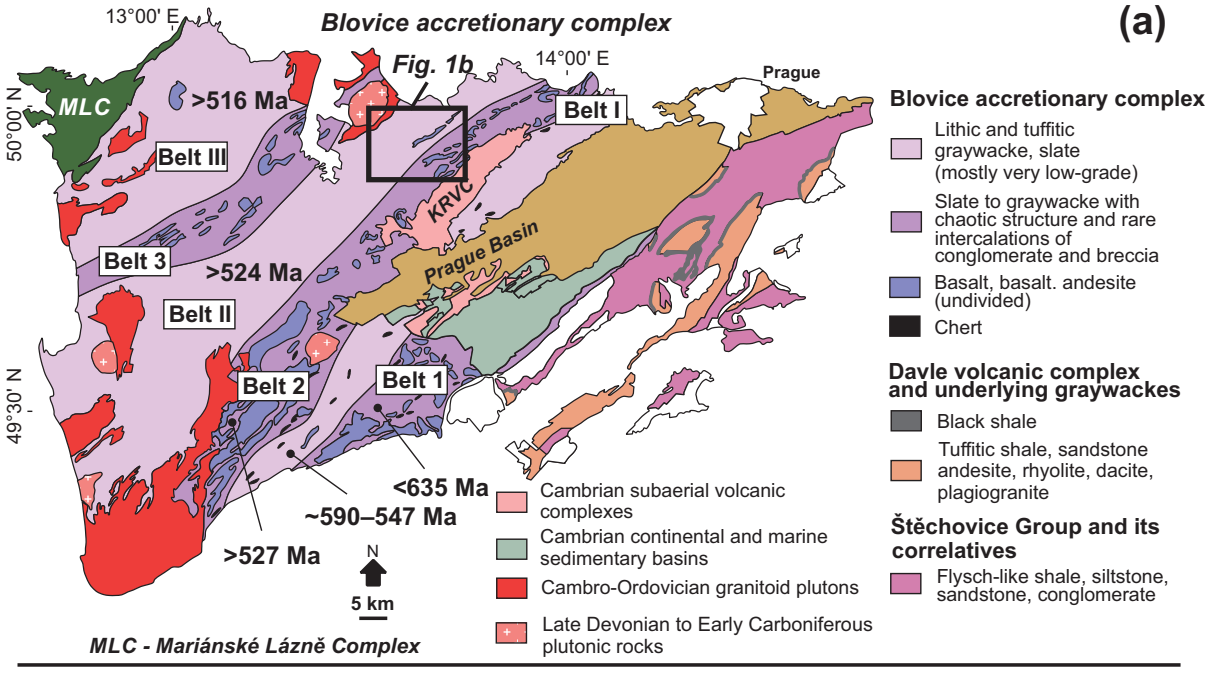
(a)
Blovice accretionary complex
13°00' E
14°00' E
50°00' N
49°30' N
Fig. 1b
Prague
MLC
>516 Ma
Belt III
Belt I
KRVC
Prague Basin
Belt 3
>524 Ma
Belt II
Belt 2
Belt 1
<635 Ma
~590–547 Ma
>527 Ma
N
5 km
MLC - Mariánské Lázně Complex
Cambrian subaerial volcanic complexes
Cambrian continental and marine sedimentary basins
Cambro-Ordovician granitoid plutons
Late Devonian to Early Carboniferous plutonic rocks
Blovice accretionary complex
Lithic and tuffitic graywacke, slate (mostly very low-grade)
Slate to graywacke with chaotic structure and rare intercalations of conglomerate and breccia
Basalt, basalt. andesite (undivided)
Chert
Davle volcanic complex and underlying graywackes
Black shale
Tuffitic shale, sandstone andesite, rhyolite, dacite, plagiogranite
Štěchovice Group and its correlatives
Flysch-like shale, siltstone, sandstone, conglomerate

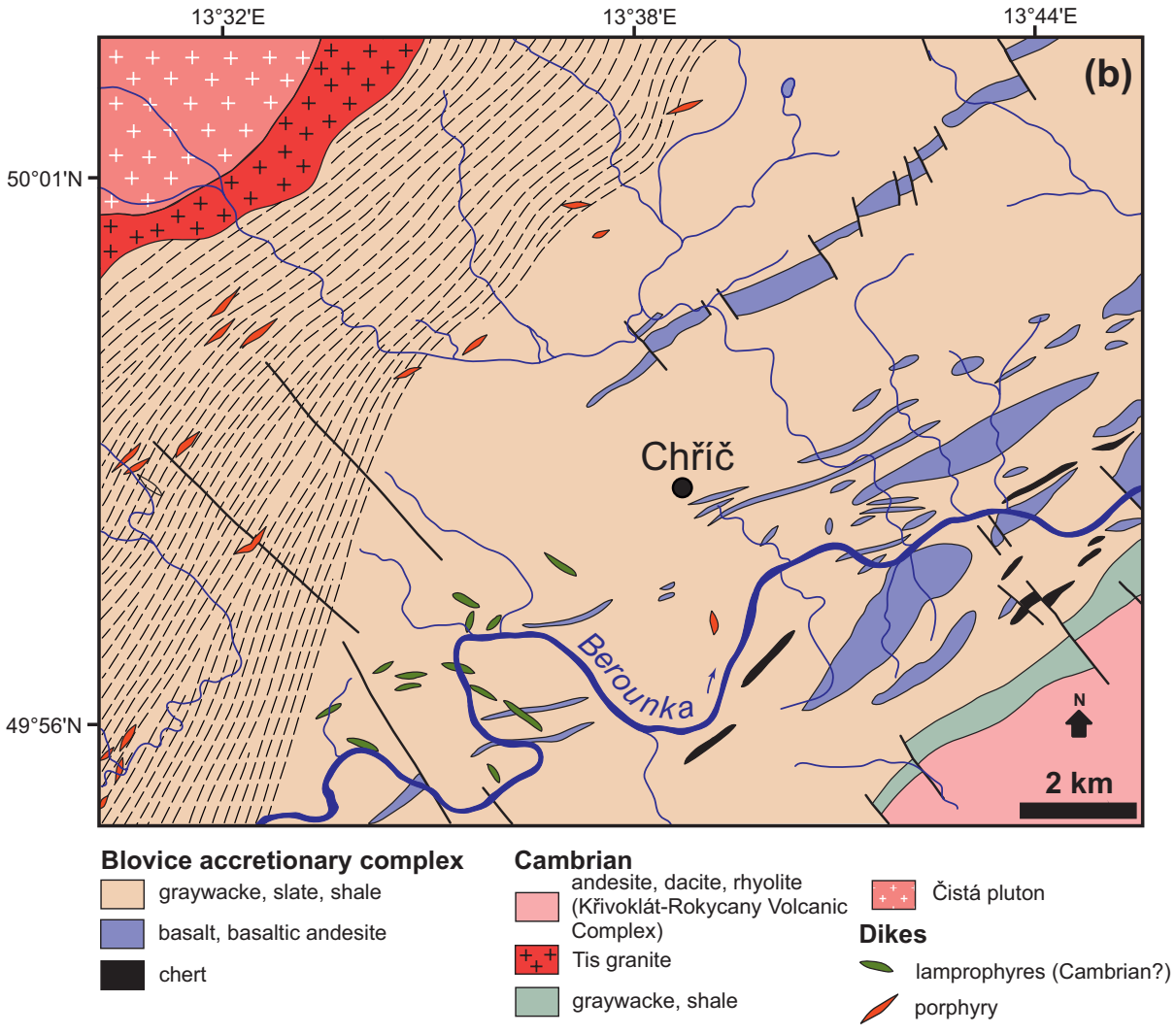
(b)
13°32'E
13°38'E
13°44'E
50°01'N
49°56'N
Chříč
Berounka
N
2 km
Blovice accretionary complex
graywacke, slate, shale
basalt, basaltic andesite
chert
Cambrian
andesite, dacite, rhyolite (Křivoklát-Rokycany Volcanic Complex)
Tis granite
graywacke, shale
Čistá pluton
Dikes
lamprophyres (Cambrian?)
porphyry

eralizations of pre-Variscan age are rather rare within the Bohemian Massif.

The TBU represents the largest of the low-grade metamorphosed basement units of the Bohemian Massif. In the current geotectonic models (e.g., Žák et al. 2020; Ackerman et al. 2022, 2023), a major part of the TBU is represented by the >600–527 Ma Blovice accretionary complex. Blovice accretionary complex formed during the subduction of an oceanic plate beneath the active margin of Gondwana in late Neoproterozoic to early Cambrian times (see also Linnemann et al. 2008; Sláma et al. 2008b; Drost et al. 2011).

The Ag–Pb–Zn and U hydrothermal vein-type ore deposits are common along the SE boundary of the TBU (e.g., Žák and Dobeš 1991), while they seem to be rather scarce within the internal part of the TBU and exhibit a different elemental association. For example, the western internal part of the TBU hosts galena–sphalerite±fluorite veins of the Stříbro Ore District (e.g., Pertold 1959; Bernard and Žák 1992; Dobeš et al. 1995, 1997) of uncertain age. Similarly, rare fluorite–barite or barite veins, usually considered to be of late Variscan or post-Variscan age, also occur within the TBU (Žák et al. 1990) but direct geochronological constrains are also missing.

In the central part of the Blovice accretionary complex, an unusual Sb-dominated mineralization near the village of Chříč (Fig. 1) always attracted the attention of ore geologists since its first detailed description provided by Katzer (1904). Recently, detailed ore mineralogy was provided by Pauliš et al. (2019) who identified stibnite, arsenopyrite and pyrite representing the major ore minerals along with other 19 subordinate or accessory ore minerals of Cu, Zn, Pb, Ag and Fe, and several gangue minerals. However, the age and the relationship to either Cadomian, Cambrian/Ordovician (e.g., Kožlany intrusive zone; Klomínský et al. 2010), Variscan or even post-Variscan tectonothermal events as well as physical and chemical conditions of ore formation have not been studied.

Therefore, this pilot study provides new constrains on the Chříč ore vein formation in terms of its mineral succession, age (Re–Os arsenopyrite, common Pb galena data), hydrothermal fluid sources and ore genesis. Using this combined information, we discuss the origin and temporal evolution of the mineralization and identify whether the formation of ore mineralization is somehow connected with local volcanosedimentary TBU successions that might serve as possible sources of carbon, sulfur and metals.

⇦

Fig. 1 Geological position of the studied Chříč ore mineralization: **a –** background local geology follows geological maps of Čepek ed. (1961) and Zoubek ed. (1964); **b –** detailed geology of the area studied. Hatched area around the outcrops of the Čistá pluton indicates the extent of metamorphic zones.

2. Local geology and ore mineralization

The Chříč mineralization is located in Belt 2 of the Blovice accretionary complex (*sensu* Hajná et al. 2013; Fig. 1). Belt 2 is dominated by siliciclastic successions (graywacke, siltstone, shale) accompanied by bodies of altered submarine basalts with MORB- or OIB-like compositions (Ackerman et al. 2019) together with occasional lenses of pyritic black shale (Pašava et al. 2021), chert (Ackerman et al. 2023) and rare impure limestone (Ackerman et al. 2022). Some of these lithologies are cropping out close to Chříč. Based on detrital zircon U–Pb ages, the maximum depositional age of Belt 2 has been estimated at ~584–527 Ma (Hajná et al. 2017; Žák et al. 2020; Pašava et al. 2021). The TBU rocks in the study area are only weakly metamorphosed in the zeolite facies or, in more distant NW surroundings of Chříč, in the prehnite–pumpellyite and greenschist facies (Cháb and Pelc 1968). Yet, we note that the metamorphic grade of the TBU lithologies generally increases in the NW direction, where the effects of Cadomian and Variscan metamorphic events overlap (see Cháb et al. 2010 for a review). The surface distance from Chříč to a zone where the effects of medium-pressure and medium-temperature metamorphism start to be more obvious, is about 5 km.

Steeply dipping dikes of mafic rocks (lamprophyre) crosscut the TBU successions, which is indicative of Paleozoic age of the dikes. They are usually up to several meters thick and penetrate the volcanosedimentary successions at several sites in the wider surroundings of Chříč (Krmíček et al. 2009). The dikes strike usually E–W or NE–SW, including a dike of amphibole lamprophyre (spessartite) several meters thick, described directly from the Sb ore exploration mine (Katzer 1904).

Whereas gravity data (e.g., Sedlák 1998) do not indicate the presence of a large granitic intrusion at a depth in the Chříč area, granitoids in the wider surroundings (~10 km away) are represented by late Cadomian to post-Cadomian and Variscan intrusions of the Čistá pluton, which has a two-phase evolution. The older phase is represented by the Tis granite with a laccolith shape of Cambrian age (~505 Ma; Venera et al. 2000), the younger Čistá granodiorite–tonalite penetrating the Tis granite is of Devonian age (373 ± 1 Ma; Venera et al. 2000; see also Žák et al. 2011; Deiller et al. 2021). Furthermore, in the surroundings of Chříč, several "microgranite" (aplite) dikes were identified (Blažek et al. 1996; Vorel et al. 2012).

The long history of mining in the Chříč area has been summarized elsewhere (Rožmberský 2010; Pauliš et al. 2019). In brief, it started with the processing of pyritic black shales for the production of so-called Bohemian fuming sulfuric acid in the late 18th and in the 19th centuries. In fact, the black shale prospection led to the first

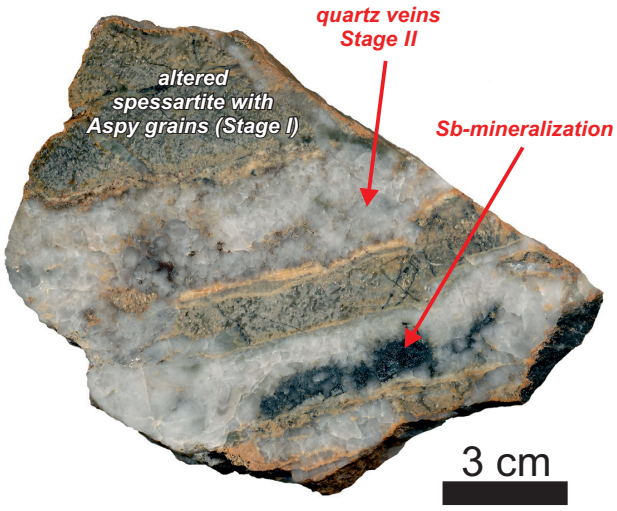

Fig. 2 A typical texture of ore fill from Chříč with evidence of brecciation. Fragments of altered spessartite with arsenopyrite in altered rock are rimmed by yellow carbonate veinlets (Stage I), then fragmented and cemented by coarsely crystalline quartz. Stibnite forms dark-colored cluster in the quartz.

discovery of Sb ore at Chříč in 1856. An exploration shaft (Josefi Shaft; WGS 84 coordinates: 49.96847°N, 13.65217°E) was opened and subsequently deepened. Its drives were extended several times in the period from 1858 to 1937, with a final depth of the mine reaching 16 m and the total production of high-grade Sb ore up to few tens of tons only. The prospect was eventually abandoned after World War II due to low proved ore reserves.

The most detailed description of the position of the ore vein was given by Katzer (1904). According to his description, morphologically complex hydrothermal quartz–carbonate vein with sulfidic minerals occurs either in the internal part of the altered lamprophyre (spessartite) dike or follows its contact. The country rocks adjacent to the spessartite dike are contact-metamorphosed, tectonically affected with brecciation and strongly hydrothermally altered and silicified. The main ore vein strikes E–W (90–105°) with a steep dip (80°) to the N and a thickness of up to 1.5 m in the exploration shaft. The thickness of the side-branches, separated from the main vein by a 1.5 m thick silicified zone, was reaching up to 0.5 m.

The major ore mineral is represented by stibnite, occurring in the form of irregular veinlets and clusters up to 10 cm thick, accompanied by minor pyrite and arsenopyrite and other 19 subordinate or accessory Cu, Zn, Pb, Ag and Fe ore minerals (Pauliš et al. 2019; see also Figs 2, 3). Stibnite is compact, fine-grained or consisting of radial or straw-like elongated grains that are generally devoid of other mineral inclusions. Irmler (1915) reported notably high Ag and Au contents (36 and 16 g/t, respectively) in a quartz–arsenopyrite sample from Chříč, but this was not confirmed by subsequent measurements.

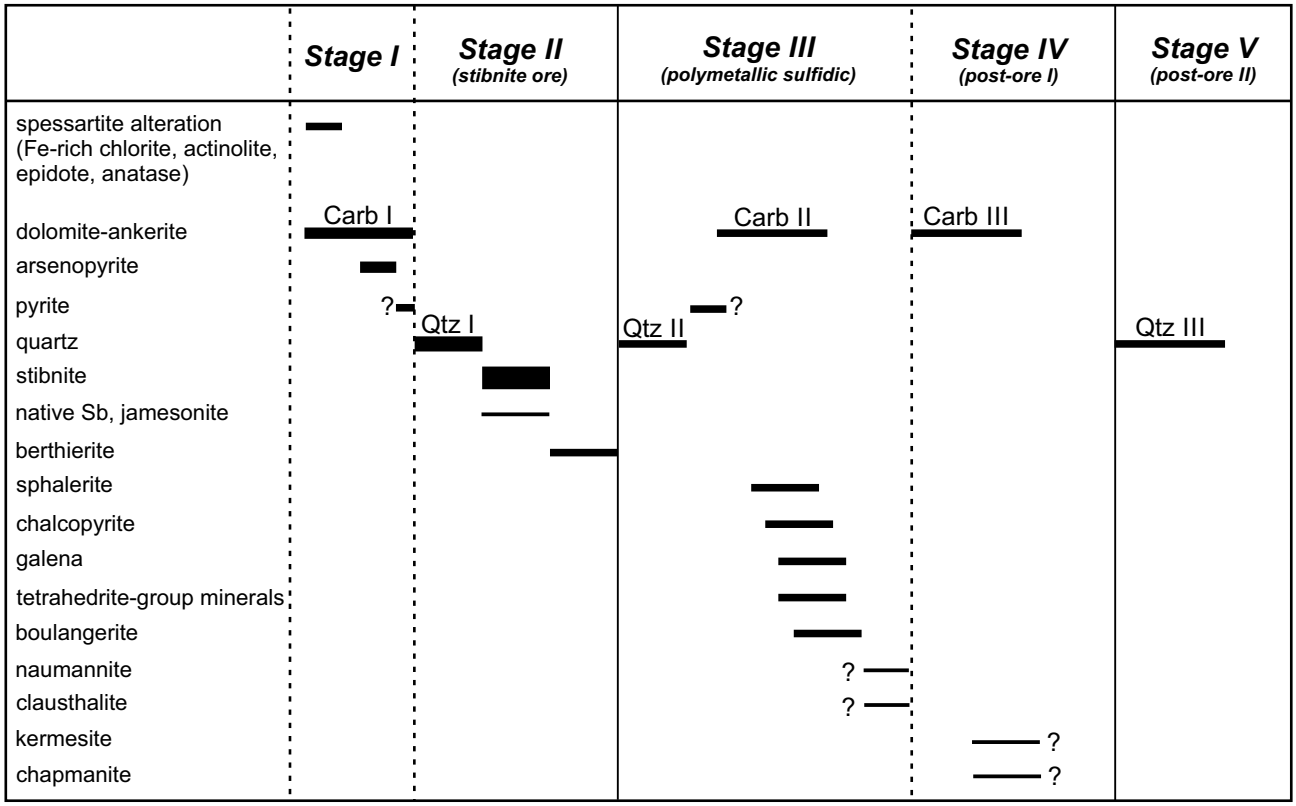

Fig. 3 A schematic succession of hydrothermal stages. Dashed lines – brecciation of earlier hydrothermal stages.

Nevertheless, Malec and Novák (1982) identified three types of gold grains with variable fineness in the fluvial sediments of the Chříč Creek, one of them being interpreted as of a local origin. Apparently, Au-bearing quartz veins within the Neoproterozoic black shale formations have been reported from several places of the TBU (e.g., Pašava et al. 2023) with the closest one located about 4.5 km SW of Chříč in the vicinity of Hřešihlavy (Zimmerhakl 1982), suggesting a possible relationship.

3. Methods

Mineralogy of vein filling and the succession of hydrothermal events have been first determined using field observation and a study of samples under a binocular microscope. Subsequently, polished sections were examined by reflected light microscopy and Electron Probe Microanalysis (EPMA) using the FE-SEM Tescan Mira3 GMU fitted with an Oxford Instruments X-Max 80 EDS detector housed at the Czech Geological Survey (CGS). A set of synthetic elemental and mineral standards was used for the analysis, with analytical conditions as follows: 15 kV accelerating voltage, 3 or 40 nA probe current depending on work distance and 40 s counting time for peaks.

The proportion of carbonate phases in the mineral separates prepared for C and O isotope analyses was determined by XRD technique (Bruker D8 Advance) at the CGS. Gold content of bulk ore samples was determined after sample decomposition by ICP MS Agilent 7900 also in the CGS laboratories. Pyrite, arsenopyrite, boulangerite, stibnite, sphalerite and galena mineral separates were prepared by a combination of hand picking from crushed specimens and physical methods. The purity of mineral separates was better than 90% in most cases.

Lead isotopic composition of galena separates was acquired at the Institute of Geology of the Czech Academy of Sciences (IG CAS). About 0.6–0.9 mg of galena powder was dissolved using 1 ml of aqua regia on the hot place for 24 hours at 130 °C. Subsequently, the samples were dried, re-dissolved in 7 M HNO_3, dried again and finally dissolved in 1 M HNO_3. Lead was isolated from the matrix by ion exchange chromatography using Sr resin (Triskem) and 2 ml of 6 M HCl for Pb collection (Pin et al. 2014). The isotopic analysis of Pb was carried out using the Triton Plus thermal ionization mass spectrometer (TIMS; ThermoFisher Scientific), housed at the IG CAS using the methods specified in Ackerman et al. (2020).

Rhenium-Osmium (Re-Os) geochronology was performed at University of Alberta. Aliquots of each arsenopyrite-dominated mineral separate were weighed and dissolved at 220 °C for 48 hours in reverse aqua regia in Carius tubes along with a conventional ^{185}Re–^{190}Os spike. Afterwards, chemical separation and purification of Os and Re followed the procedures given in Shirey and Walker (1995), Cohen and Waters (1996) and Birck et al. (1997), as described in detail by Morelli et al. (2005). Total procedural blanks for Re and Os were < 3 and 0.1 pg, respectively (< 0.01 picograms ^{187}Os).

Zircons from fluvial sediments of local creek below the ore occurrence were also studied. Prior their U–Pb dating, the internal textures of zircons were studied. The cathodoluminescence (CL) images were acquired with the field emission gun electron probe microanalyzer JXA-8530F equipped with a panchromatic CL detector at the Institute of Petrology and Structural Geology (Faculty of Science, Charles University, Prague) under the conditions of 15 kV accelerating voltage and 30 nA probe current. The U–Pb zircon dating and in-situ trace element data for sulfides were obtained using ThermoScientific Element 2 sector field ICP–MS coupled to a 193 nm ArF excimer laser system (Teledyne/Cetac Analyte Excite laser) at the IG CAS following the methods specified in Pašava et al. (2021) and Žák et al. (2022), respectively. During the course of this study, zircon reference material 91500 was used as isotopic calibration primary standard for normalization while zircon reference materials GJ-1 and Plešovice PL-1 were used for the method validation. The obtained ages for 91500 (1063 ± 2 Ma; 2σ), GJ (607 ± 2 Ma; 2σ) and PL-1 (340 ± 1 Ma; 2σ) correspond well within 1% uncertainty with respect to the reference values (Wiedenbeck et al. 1995; Jackson et al. 2004; Sláma et al. 2008a). Sulfide trace element data were calibrated using the MASS-1 sulfide (USGS) with ^{57}Fe being used as the internal standard assuming its concentration based on arsenopyrite stoichiometry. Glass reference material NIST SRM 610 was used as a reference standard. The precision of the laser ablation analyses (as a relative 1 sigma error – RSD) ranges between 5 and 15 % for most of the detected elements.

Fluid inclusions (FI) in minerals of quartz–dolomite-ankerite–sulfidic vein were studied by means of optical microthermometry by Chaixmeca equipment (Poty et al. 1976) at the CGS. The apparatus was calibrated for temperatures between –100 and +400 °C using chemical standards of the Merck Company, water–ice melting temperature, and by phase transitions in FI with pure CO_2. Standard measurements indicate the reproducibility of ±0.2 °C at temperatures below 0 °C and ±3 °C at temperatures up to 400 °C. The salinity of the aqueous FI was recalculated according to Bodnar and Vityk (1994). The density and composition of inclusions with CO_2 and CH_4 were recalculated according to Bakker and Diamond (2000) and Van den Kerkhof and Thiery (2001). Phase changes in the inclusions were detected during micro-

scopic observations and recorded by measurements of the following temperatures: $TmCO_2$ – temperature of melting of solid CO_2, $ThCO_2$ – temperature of homogenization of CO_2, to liquid or to vapor, Tm_{clat} – temperature of melting of the clathrate, Th –temperature of bulk homogenization, to liquid or to vapor, Tm – temperature of melting of the last ice crystal. The micro-Raman analyses of fluid inclusions were performed at IG CAS using a Raman micro-spectrometer S&I MonoVista CRS+.

The C–O stable isotope compositions of carbonates were determined at the CGS using a conventional carbonate decomposition by 100% H_3PO_4 under vacuum at 25 °C (McCrea 1950) followed by the measurement of the released CO_2 gas using a Finnigan Delta V mass spectrometer. The reaction time was extended to 24 hours to obtain a full reaction yield. Since the studied carbonates belong to the dolomite-ankerite solid solution, all $\delta^{18}O$ data have been corrected by subtraction of 0.84 ‰ (Friedman and O'Neil 1977). The overall analytical uncertainty was ±0.15 ‰ for both $\delta^{13}C$ and $\delta^{18}O$ values.

Sulfur isotope compositions of sulfide minerals were determined at the CGS using direct oxidation by CuO under vacuum (Grinenko 1962) followed by cryogenic purification of the prepared SO_2 gas and measurement of sulfur isotope data on a Finnigan MAT 251. The overall analytical uncertainty of $\delta^{34}S$ was ±0.3 ‰.

4. Results

4.1. Mineralogy, texture and succession of magmatic and hydrothermal events

During the lamprophyre (spessartite) dike intrusion, surrounding black shales were metamorphosed at the dike contact. However, the black shales are also present in the form of up to cm-sized fragments embedded within spessartite matrix, or were almost completely consumed by the lamprophyric melt, being converted to black streaks or veinlets containing variable proportions of migrated carbonaceous matter. Spessartite contains plagioclase laths, amphibole, pyroxene and ilmenite here. Large-scale alteration is indicated by serpentine replacing olivine, leucoxene after ilmenite, and the presence of a fine-grained mixture of Fe-rich chlorite, actinolite and epidote in the matrix.

The studied samples of hydrothermal vein fill document repeated pulses of hydrothermal fluids, separated in some cases by tectonic movements and brecciation of older vein fill. The sequence of hydrothermal events started by the alteration of spessartite (Figs 2, 3).

Hydrothermal history can be divided into five mineralization stages (Fig. 3): (1) Early stage (***Stage I***) characterized by the formation of carbonates (dolomite-ankerite series; Carb I), arsenopyrite and possibly also pyrite, (2) Sb stage (***Stage II***) with abundant quartz (Qtz I) accompanied by the formation of stibnite ± berthierite, native Sb and jamesonite, (3) polymetallic (Cu–Pb–Zn–Ag) stage (***Stage III***) with several sulfidic minerals, dolomite-ankerite II and quartz (Qtz II), (4) post-ore stage I (***Stage IV***) characterized by the formation of dolomite-ankerite III, and (5) post-ore stage II (***Stage V***) with the third generation of quartz (Qtz III).

Stage I is represented by widespread carbonatization of spessartite that resulted in a replacement of mafic minerals by carbonates of the dolomite-ankerite series accompanied by the formation of Fe-rich chlorite, actinolite and epidote, conversion of olivine to serpentine minerals and abundant ilmenite to anatase. Small idiomorphic columnar arsenopyrite grains were formed during this stage, followed by dolomite-ankerite veinlets. Anhedral leucoxene and sometimes also pyrite inclusions are enclosed in some arsenopyrite grains. Pyrite is most probably also present in Stage I. Pyrite generations are, with respect to the massive appearance of the ore fill and repeated brecciation, difficult to identify and distinguish from each other.

Stage II started with strong brecciation, followed by cementation by coarse-crystalline quartz (Qtz I), which rarely contains minor cavities. The main Sb-ore mineral, stibnite, precipitated between the quartz crystals, also forming veinlets along quartz veins or mono-mineral veinlets in cracks in spessartite. Furthermore, stibnite also rarely forms acicular crystals in quartz cavities. Stibnite rarely contains inclusions of native antimony and of jamesonite (Pauliš et al. 2019) and is frequently accompanied by relatively younger berthierite, which commonly rims stibnite aggregates.

Stage III is characterized by the formation of veinlets of dolomite–ankerite (Carb II), locally with small cavities, which contain mm-sized grains of sphalerite, chalcopyrite, galena and needles of boulangerite replacing galena. Some sphalerite grains contain small inclusions of galena and an Ag-rich mineral of the tetrahedrite group. Crystals of relatively rare galena commonly display skeletal character and grow together with chalcopyrite, the Ag-rich mineral of the tetrahedrite-group mineral or boulangerite. Sometimes, galena fills tiny cracks in dolomite–ankerite. Rarely occurring selenides such as naumannite and clausthalite most probably belong a late part of the same mineralization stage.

Younger veins of finely crystalline carbonate of dolomite–ankerite series (Carb III) that fill open cracks represent ***Stage IV*** while the termination of the hydrothermal processes is marked by the formation of late quartz veinlets (Qtz III, ***Stage V***). Pyrite is generally abundant and can be found in the whole mineralized rock. It is, however, difficult to recognize whether it rep-

resents a remnant of black shale fragments or a product of ***Stage I*** or ***Stage III*** mineralization. Late low-temperature alteration processes are characterized by the formation of kermesite and chapmanite. Among supergene minerals, cerussite, anglesite, pyromorphite, valentinite, jarosite and abundant *limonite* were identified (see Pauliš et al. 2019 for details on mineralogy).

Tab. 1 Lead isotope compositions of the Chříč galena

Sample No.	$^{206}Pb/^{204}Pb$	2SE	$^{207}Pb/^{204}Pb$	2SE	$^{208}Pb/^{204}Pb$	2SE
Pb #1 CH-10	18.082	0.0028	15.574	0.0024	37.890	0.0058
Pb #2 CH-16	18.079	0.0009	15.564	0.0007	37.831	0.0018
Pb #3 CH-22	18.074	0.0026	15.577	0.0022	37.881	0.0056

4.2. Gold concentrations and occurrence

Gold particles were not detected in any of the studied polished samples. This is compatible with the low contents of 595, 180 and 100 ppb Au in three analyzed samples of ore fill with disseminated arsenopyrite and pyrite. Furthermore, laser ablation analyses (ESM 1) confirmed Au contents in arsenopyrite in the range of 0.5–173 ppm (median 27 ppm) that are correlated with Se (r = 0.97). Arsenopyrite also contains Sb (0.6–2.4 wt. %, median 1.5 wt. %). Au contents in associated pyrite range from 1 to 33 ppm (median 9 ppm) and correlate with As (r = 0.75), which is extremely variable (0.1–5.7 wt. % As, median 3.7 wt. %). The extremely low median Au/As values in pyrite (~0.0002) indicate that Au is present in the form of a solid solution (Reich et al. 2005).

The presence of gold in stream sediments immediately below the ore occurrence was confirmed by Malec and Novák (1982). Therefore, we studied a new heavy mineral concentrate from fluvial sediments of the Chříč Stream immediately downstream of the ore occurrence. The heavy mineral association of the sample was found to be dominated by ilmenite, magnetite and arsenopyrite, while limonite represented a minor component. More rarely, pyrite, zircon and pyroxene were also present while cassiterite, rutile, titanite, staurolite, corundum, kyanite, cerussite and native gold represented accessory minerals.

Based on their chemical composition and shape, the obtained gold particles can be subdivided into three types. Strongly abraded and reworked oval, flat gold particles up to 0.16 mm thick (***Type I***) consist of pure gold (Ag up to 1 wt. %, Hg below EPMA detection limit). The second type (***Type II***) is represented by flat, elongated gold particles up to 0.2 mm thick, showing an irregular surface zone up to 20 μm thick, containing 2–3 wt. % Ag. Their internal parts contained 16–25 wt. % Ag (other elements were below EPMA detection limit). ***Type III*** consists of irregular jagged gold particles which were clearly subjected to almost no fluvial transport. They contain 23 wt. % Ag, 0.2 wt. % Hg, and show no zones with secondarily purified gold of higher fineness. Short, up to 2 μm thick veinlets of gold containing up to 2 wt. % Hg were observed inside these gold particles and also on their surfaces.

4.3. Lead isotopic compositions of galena

Lead isotope compositions of galena from Chříč (average isotope ratios $^{206}Pb/^{204}Pb$ 18.078; $^{207}Pb/^{204}Pb$ 15.571, $^{208}Pb/^{204}Pb$ 37.868; see Tab. 1) are similar to those reported for some Variscan Ag–Pb–Zn±Sb hydrothermal vein mineralizations of the Bohemian Massif (Vaněček et al. 1985), e.g., the Příbram ore district ($^{206}Pb/^{204}Pb$ 18.02, $^{207}Pb/^{204}Pb$ 15.53–15.57, $^{208}Pb/^{204}Pb$ 38.03–38.17) or the Kutná Hora ore district ($^{206}Pb/^{204}Pb$ 18.09, $^{207}Pb/^{204}Pb$ 15.59, $^{208}Pb/^{204}Pb$ 38.21). In contrast, galena lead isotope ratios from the Stříbro ore district located within the TBU are significantly different ($^{206}Pb/^{204}Pb$ 18.50, $^{207}Pb/^{204}Pb$ 15.50, $^{208}Pb/^{204}Pb$ 38.67). Similarly, the Chříč lead isotope ratios are also somewhat different from those reported for the nearby Variscan Hůrky polymetallic vein mineralization (molybdenite Re-Os age of 377 ± 2 Ma; Ackerman et al. 2017) with $^{206}Pb/^{204}Pb$ of 18.28, $^{207}Pb/^{204}Pb$ of 15.62 and $^{208}Pb/^{204}Pb$ of 38.32 (Vaněček et al. 1985).

Vaněček et al. (1985) also reported one Pb isotope galena value from Chříč ($^{206}Pb/^{204}Pb$ 18.14, $^{207}Pb/^{204}Pb$ 15.58, $^{208}Pb/^{204}Pb$ 38.01), which is somehow more radiogenic than our new determinations.

Tab. 2 Re-Os isotope compositions of arsenopyrite separates from Chříč

Sample / fraction	Re (ppb)	2s	Os (ppt)	2s	$^{187}Re/^{188}Os$	2s	$^{187}Os/^{188}Os$	2s	Model Age (Ma)
CH31	2.372	0.012	15.0	5.5	4553	1406	38.2	11.8	494 ± 6
CH31-R	2.620	0.010	18.3	2.2	2925	325	24.9	2.8	499 ± 4
CH33	4.050	0.012	25.7	9.2	13542	3631	129.0	34.7	567 ± 12
CH33-R	4.145	0.013	26.2	6.1	8585	1552	78.9	14.3	546 ± 8
CH15	2.437	0.009	18.1	1.9	2752	257	25.1	2.4	533 ± 13
CH15-R	2.415	0.011	17.8	3.1	2902	451	26.6	4.1	537 ± 4
CH25	1.872	0.008	12.2	4.3	6174	1732	56.5	15.9	542 ± 10
CH27	2.882	0.010	19.7	2.1	3342	308	28.7	2.7	505 ± 9

4.4. Arsenopyrite Re–Os dating

Results of the Re–Os isotopic analyses of arsenopyrite from Stage I of the hydrothermal mineralization (the only arsenopyrite generation at Chříč) are given in Tab. 2, with the corresponding Re–Os regression being plotted in Fig. 4 using IsoplotR (Vermeesch 2018). All data combined do not yield a plausible age because the data clearly define two arrays on a Re-Os diagram, with five of 8 analyses defining a regression with an age of 557 ± 26 Ma. Three analyses plot below this ca 557 Ma regression, yielding a younger age of 488 ± 23 Ma.

4.5. U–Pb zircon geochronology

Some zircon grains recovered from the heavy mineral concentrate of the Chříč Stream are almost devoid of abrasion, which might indicate their short fluvial transport. Thus, two size subsets of zircon populations (subsamples CH-46A and CH-46B) from the same heavy mineral concentrate, slightly differing only in their grains size, were analyzed for their U–Pb ages using LA-ICP-MS technique (see ESM 2 for data). The purpose of the analyses was to get a general view on magmatic and sedimentary processes at the site.

Subsample *CH-46A* contains zircons which are mostly prismatic stubby subhedral grains (or their fragments) 150–450 μm long, with sector or oscillatory/planar zoning or with commonly unzoned cores in cathodoluminescence (CL; Fig. 5). A total of 56 analyses group into three major age clusters (Carboniferous, Cambrian, and Neoproterozoic) and a single inherited ~2.0 Ga Paleoproterozoic age record. The Carboniferous spectra yielded a concordia age of 330 ± 3 Ma (2σ, n = 14) while most of the grains (n = 39) yielded Cambrian concordia age peak of 501 ± 3 Ma (2σ), with two grains showing Ediacaran age of 604 ± 6 Ma (2σ, n = 2) (Fig. 6, ESM 2).

Subsample *CH-46B* contains prismatic to isometric and mostly euhedral zircons with a length of 150–350 μm. In the CL, they are oscillatory/planar zoned, often with sector zoning, and most of the grains display weakly zoned, patchy or unzoned cores. The zircon population defines two major age groups: (1) a younger Carboniferous age group (n = 13) with age spectra in the range of c. 320–345 Ma (2σ) and the concordia age of 328 ± 6 Ma, and (2) an older wide cluster (n = 32) with ages ranging between 461 and 556 Ma and the Cambrian concordia age of 500 ± 6 Ma (2σ). Besides, also a maximum at c. 596 Ma and a Paleoproterozoic cluster between 1.9 and 2.5 Ga were recorded.

In summary, the two subsamples yielded almost identical age spectra and exhibited uniform magmatic Th/U ratios with an average value of ~0.5 (ESM 2).

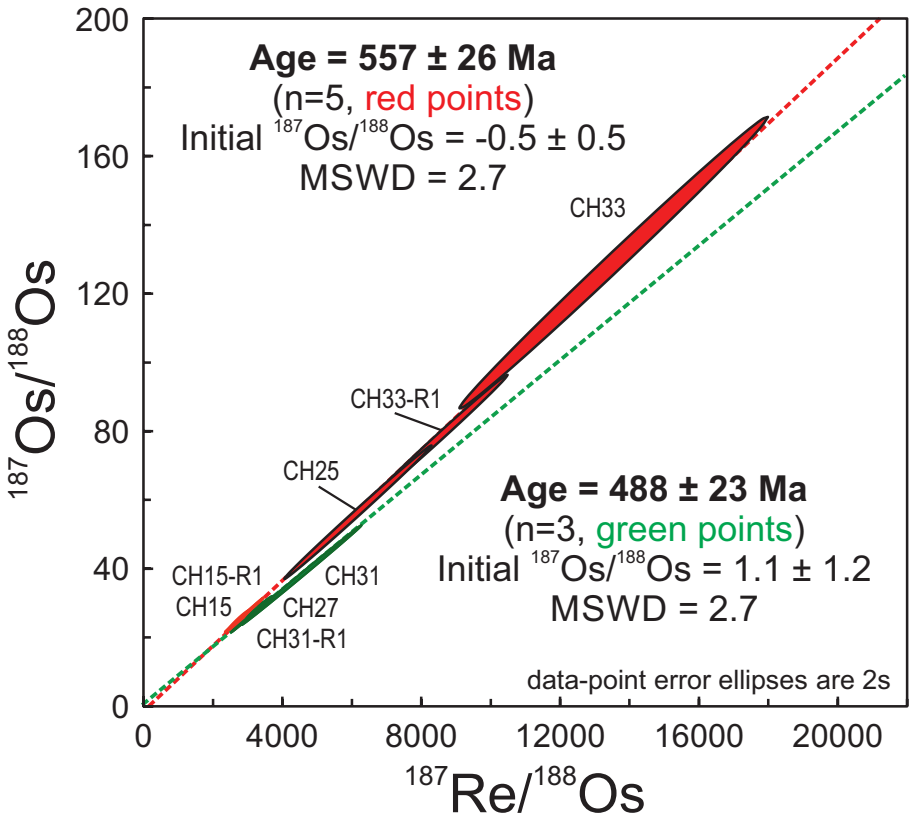

Fig. 4 Results of Re–Os arsenopyrite dating.

4.6. Fluid inclusion study

Fluid inclusions were first studied at a room temperature to identify individual populations (Goldstein and Reynolds 1994), their relationships to the host mineral (primary, pseudosecondary or secondary types) and the shape, the size and the degree of filling, i.e., the liquid-to-vapor ratio (LVR = L/(L + V)). The obtained fluid inclusion data are contained in Tab. 3.

Fluid inclusions were measured in quartz II, carbonate of dolomite-ankerite series and sphalerite of the Stage III, in minerals with tight connection to sulfides of the polymetallic

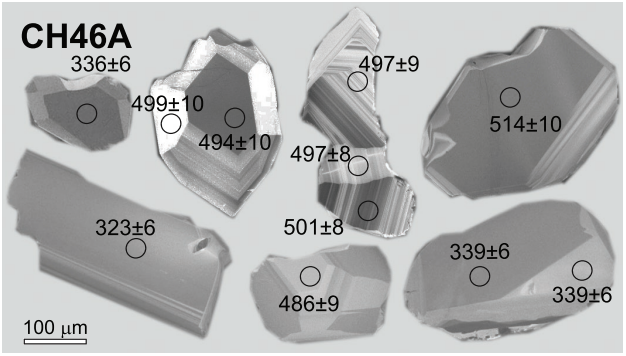

Fig. 5 CL images of the studied zircons with analyzed areas and ages.

stage. Qtz II was presented in two types, massive Qtz II with carbonate of dolomite-ankerite series and sulfides along fractures, and fine-grained crystalline quartz enclosing fragments of older veins, sulfide minerals or rocks (breccia-type texture). Both types of quartz contained the H_2O–CO_2 type of inclusions.

Primary two- or three-phase H_2O–CO_2 inclusions with variable LVR from 0.4 to 0.8 were observed in massive Qtz II. The inclusions have various shapes and sizes from ~5 to 20 µm in diameter, and their $TmCO_2$ occurred between –57.2 and –58.6 °C, indicating a small admixture of CH_4. It was proved by the analyses using micro-Raman spectrometry. The content of CH_4 reached up to 10 mole % in the gaseous phase. The $ThCO_2$ was observed both to liquid ($ThCO_2^L$ = 19.5 to 28.7 °C) and to vapor ($ThCO_2^V$ = 13.6 to 29.3 °C). Therefore, the densities of the gaseous phase range from 0.14 to 0.78 g/cm^3. The Th were observed both to the liquid (Th^L = 258 to 349 °C) and to the vapor phase (Th^V = 295 to 330 °C; Fig. 7). Temperatures of melting of clathrate (Tm_{clat}) were measured between 3.9 and 9.2 °C, suggesting the salinity of aqueous fluid in a wide range of 1.8 to 10.9 wt. % NaCl eq.

Similar primary two- or three-phase H_2O–CO_2 inclusions with slightly different LVR from 0.4 to 0.7 were also found in Qtz II with a brecciated texture. The inclusions have various shapes and dimensions from 5 to 10 µm in diameter. The $TmCO_2$ was observed between –57.2 and –57.8 °C, indicating a small admixture of CH_4 up to 8 mole %. The homogenization of carbonic phase was measured both to liquid ($ThCO_2^L$ = 16.8 to 30.0 °C) and to vapor ($ThCO_2^V$ = 20.1 to 29.7 °C), assuming the density of the carbonic phase from 0.19 to 0.81 g/cm^3. The temperatures of total homogenization were observed both to the liquid (Th^L = 267 to 334 °C) and the vapor phase (Th^V = 326 to 334 °C). The Tm_{clat} achieved the values between 5.2 and 7.7 °C, indicating the salinity of aqueous fluid from 4.5 to 8.7 wt. % NaCl eq.

Fluid inclusions of H_2O type, probably associated with the H_2O–CO_2 inclusions, were also found in both forms of quartz II. The inclusions show various shapes, diameters of ~5 to 20 µm and LVR between 0.7 and 0.8. Their temperatures of homogenization were measured in the interval from 226 to 294 °C while the Tm values of ice were observed in the range of –0.5 to –2.8 °C, indicating low salinity values of aqueous fluid between 0.9 and 4.7 wt. % NaCl eq.

Carbonate of the dolomite-ankerite series of Stage III (Carb II; see Fig. 3) has a low transparency and contains only very small inclusions (up to 5 µm in diameter) that do not permit a collection of microthermometric data. Nevertheless, the inclusions were of two-phase type, with LVR of about 0.5.

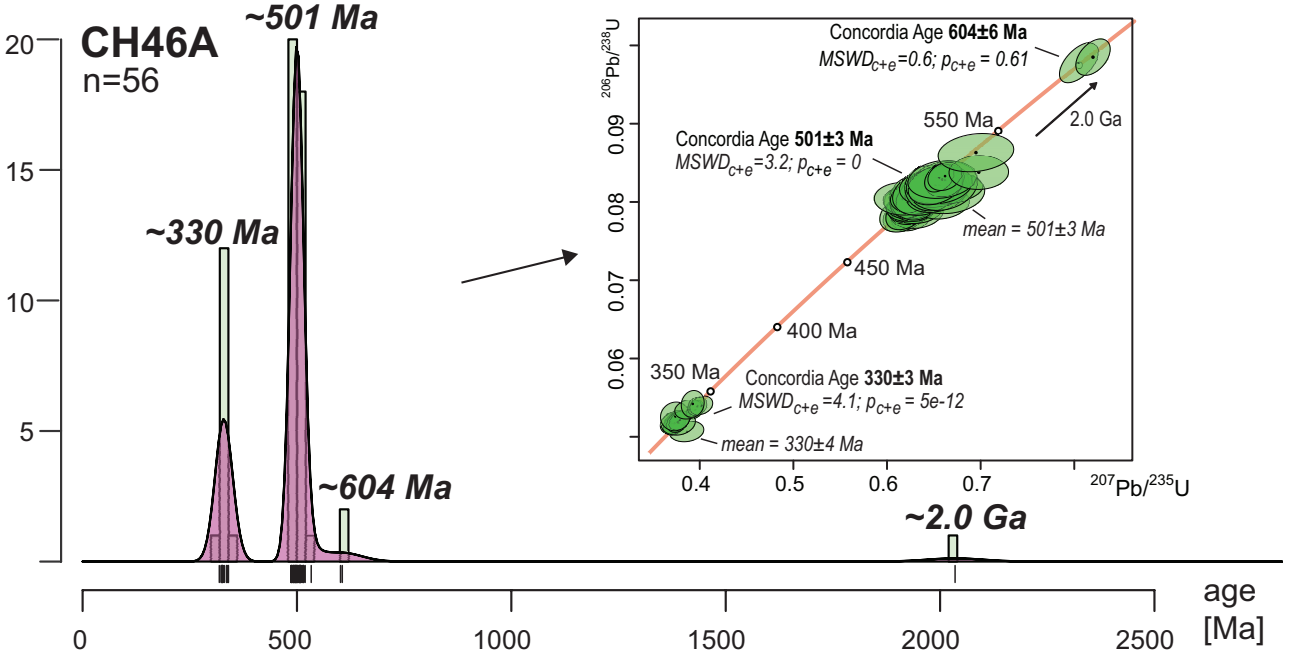

Fig. 6 Zircon U–Pb ages.

Tab. 3 Fluid inclusions data in minerals of the Chříč locality

Sample	Mineral	FI type	FIA	Size (mm)	LVR (L/L+V)	$TmCO_2$ (°C)	$ThCO_2^L$ (°C)	$ThCO_2^V$ (°C)	Tm_{clat} (°C)	Tm_{ice} (°C)	Th^L (°C)	Th^V (°C)	Salinity (mass %)
CH-01A	Qtz II – breccia type	H_2O–CO_2	primary	10	0.6	–57.8	22.8–24.2		5.2–7.1		267–324		5.8–8.7
CH-01B	Qtz II – breccia type	H_2O–CO_2	primary	10	0.7	–57.6	27.2–30	20.1–29.4	7.1–7.7		294–328	326–334	4.5–5.7
CH-02	Qtz II – breccia type	H_2O–CO_2	primary	5	0.4	–57.5		27.6–29.4					
CH-04	Qtz II – massive	H_2O–CO_2	primary	5	0.4	–57.4	27.2–28.4						
CH-05	Qtz II – massive	H_2O–CO_2	primary	10	0.7	–57.7	27.6–28.7		5.9–7.1		298–349		5.8–7.8
CH-06	Qtz II – massive	H_2O	primary	10	0.8					–1.2 to –2.8	226–268		2.1–4.7
CH-06	Qtz II – massive	H_2O–CO_2	primary	10–20	0.2–0.8	–58.4 to –58.6	19.5–28.1	27.4–28.4	8.9–9.2		258–318		1.8–2.1
CH-08	Qtz II – breccia type	H_2O–CO_2	primary	10	0.6	–57.4	26.8–29.4						
CH-10	Qtz II – massive	H_2O–CO_2	primary	10–20	0.4–0.7	–58.1 to –58.4	27.3–28.4	27.1–29.3	3.9–8.5		282–336	295–330	3.2–10.9
CH-11	Qtz II – massive	CO_2	primary	5	V only	–58.2	26.9						
CH-11	Qtz II – massive	H_2O–CO_2	primary	5	0.4	–57.2	24.8–25.4						
CH-12-1	Qtz III – post-ore quartz	H_2O	secondary	10	0.9					–2.9 to –3.8	142–158		4.8–6.2
CH-12-1	Qtz II – massive	H_2O–CO_2	primary	10	0.7	–57.2	22.5–24.7	13.6–27.6	6.2–8		272–337		4.2–6.8
CH-12-2	Qtz II – breccia type	H_2O	primary	15	0.9					–2.3 to –3.6	135–164		3.9–5.9
CH-14	Qtz II – breccia type	H_2O–CO_2	primary	10	0.7	–57.2		28.4–29.7	6.4–7.2		284–334		5.4–6.7
CH-24	Qtz II – breccia type	H_2O–CO_2	primary	5	0.4	–57.4	16.8–18.2						
CH-24-1	post-ore dolomite	H_2O	primary	10	0.9						146. 158		
CH-24-1	metamorphic quartz	H_2O–CO_2	primary	5	0.6	–57.6	4.6–9.8						
CH-29	Qtz III – post-ore quartz	H_2O	primary	10	L only					–1.2 to –3.2			2.1–5.3
CH-31	Qtz II – breccia type	H_2O	primary	15	0.7					–0.5 to –1.2	254–294		0.9–2.1

The primary inclusions in post-ore Stage V quartz (Qtz III) are mostly two-phase of H_2O type, with LVR of about 0.9 and Th values ranging from 135 to 164 °C (Fig. 7). The Tm values of ice were observed at –2.3 to –3.6 °C, indicating the salinity of the aqueous solution of 3.9–5.9 wt. % NaCl eq. Secondary inclusions are also of H_2O type, with Th values ranging from 142 to 158 °C. Temperatures of melting of ice were measured in the interval from –2.9 to –3.8 °C, which corresponds to the salinity of the aqueous solution between 4.8 and 6.2 wt. % NaCl eq.

The aqueous inclusions also occurred in the late carbonate of the dolomite-ankerite series (Carb III) of Stage IV. They showed variable shapes and degrees of filling, and their Th values were measured only in two inclusions (Th 146 and 158 °C, Fig. 7).

Single-phase, liquid-only aqueous inclusions were also found in late post-ore massive quartz III of Stage V. Temperatures of melting of ice were observed in the range from –1.2 to –3.2 °C, indicating the salinity of the aqueous fluid between 2.1 and 5.3 wt. % NaCl eq.

4.7. Carbon and oxygen isotope compositions of carbonates

Carbon and oxygen isotope compositions of carbonate of dolomite-ankerite series (Carb II) from Stage III (see Pauliš et al. 2019 for carbonate chemistry) plot in a limited area in the $\delta^{13}C$ vs $\delta^{18}O$ diagram (Fig. 8; Tab. 4) while we note that a minor admixture of earlier carbonates (Carb I) from Stage I can be also present. In comparison, younger carbonates of Stage IV (Carb III) are clearly distinguished by higher $\delta^{18}O$ values (~ –6 ‰ V-PDB; Fig. 8). Calculation of the $\delta^{18}O_{fluid}$ values of the Stage III (based on carbonate $\delta^{18}O$ and FI Th values) is not significantly affected by the selected oxygen–water isotope fractionation equation (dolomite–water oxygen isotope fractionation at 300 °C is ~6.0 ‰ after Zheng 1999, ~5.4 ‰ after Golyshev et al. 1981, or ~6.4 ‰ after Horita 2014). Similarly, neither the carbonate chemistry (within the dolomite-ankerite series) would impose a serious effect. If the temperature of dolomite-ankerite formation is set to ~ 300 °C and the carbonate–fluid oxygen isotope fractionation is approximately 6 ‰, then the $\delta^{18}O$ value of fluid would be around +7.5 ‰ V-SMOW. Therefore, it can be assumed that hydrothermal fluids of Stage III were of high-$\delta^{18}O$ type, i.e., fluids that isotopically equilibrated with hot magmatic or metamorphic rocks similar to those reported for Au–Sb ores of the Krásná Hora District by Němec and Zachariáš (2018). Both the temperature (based on FI data) and the calculated $\delta^{18}O_{fluid}$ were decreasing during post-ore Stages IV and V at Chříč.

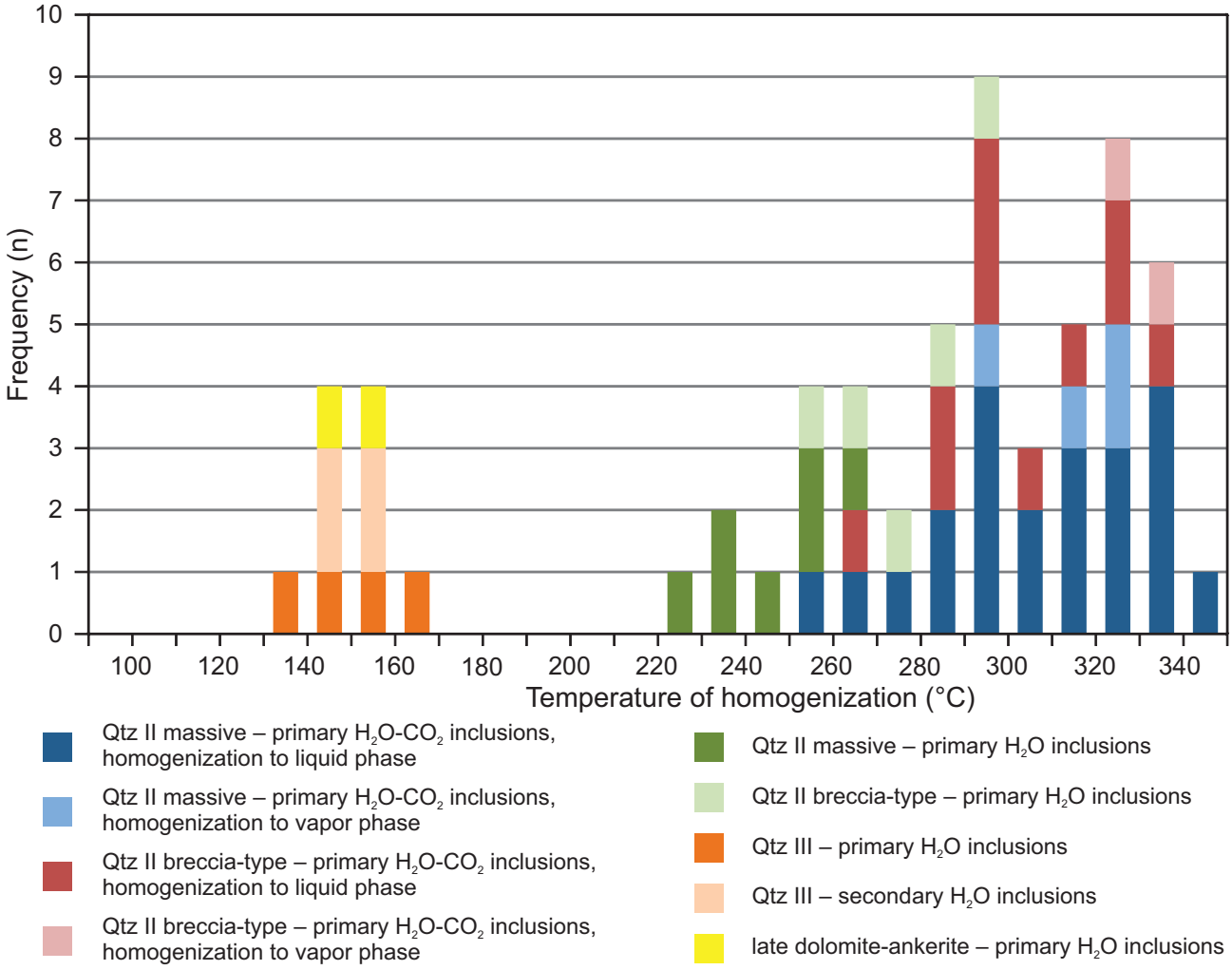

Fig. 7 Histogram of temperatures of homogenization of fluid inclusions in minerals of the Chříč locality.

All studied carbonates show low $\delta^{13}C$ values in the range from –12.2 to –15.6 ‰ V-PDB (Fig. 8) irrespective of the stage they were formed in. As the CO_2–carbonate carbon isotope fractionation is not large at temperatures in the range 300–250 °C (Ohmoto and Rye 1979), we assume also similar $\delta^{13}C_{fluid}$ indicating a significant proportion of CO_2 in the hydrothermal fluids which was derived from oxidation or thermal decomposition of organic matter.

4.8. Sulfur isotope compositions

Sulfur isotope compositions for individual sulfide fractions from Stages I, II and III are listed in Tab. 5. The distribution of $\delta^{34}S$ data is obviously bimodal with a large group of samples having $\delta^{34}S$ values in the range from –3 to –10 ‰ V-CDT irrespective of the mineral analyzed and a group of samples tending to more negative $\delta^{34}S$ values down to ~ –18 ‰ V-CDT. The widest variability of $\delta^{34}S$ values can be recognized in pyrite but it is not

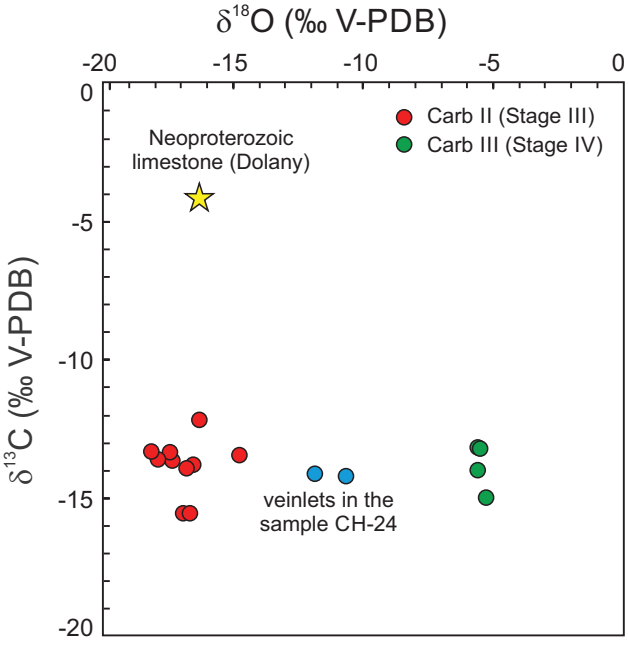

Fig. 8 Carbonate $\delta^{13}C$ and $\delta^{18}O$ data.

Tab. 4 Carbon and oxygen isotope compositions of carbonates of the dolomite-ankerite series from Chříč

Sample	$\delta^{13}C$ (‰ V-PDB)	$\delta^{18}O$ (‰ V-PDB)	$\delta^{18}O$ (‰ V-SMOW)	dolomite-ankerite proportion in analyzed sample vol. %
Ch-5	–12.2	–16.27	14.14	26
Ch-9	–13.4	–18.14	12.21	100
Ch-10	–13.6	–17.91	12.45	83
Ch-12A	–13.7	–17.35	13.02	22
Ch-12B	–13.4	–17.44	12.93	69
Ch-13	–14.0	–5.61	25.13	98
Ch-17	–15.6	–16.69	13.70	48
duplicate	*–15.6*	*–16.86*	*13.53*	
Ch-22	–13.8	–16.50	13.90	70
Ch-24 A	–13.2	–5.49	25.25	96
duplicate	*–13.2*	*–5.58*	*25.15*	
Ch-24 B	–14.2	–10.68	19.91	75
Ch-24 C	–14.1	–11.86	18.68	84
Ch-31	–13.5	–14.78	15.67	39
Ch-38	–14.0	–16.75	13.64	38
Dolany limestone	–4.2	–16.27	14.14	

Values related to the V-SMOW have been recalculated from the measured data
Proportion of carbonate of the dolomite-ankerite series is based on XRD data of the samples used for stable isotope analyses. The rest are non-carbonate minerals.

feasible to relate this feature to possible different pyrite generations. The tested mineral pairs of sphalerite–galena and pyrite–galena are not in sulfur isotope equilibrium, probably due to a non-simultaneous deposition of these sulfidic minerals. Therefore, sulfur isotope thermometers could not be applied.

5. Discussion

5.1. Formation of ore mineralization and the gold origin

It appears from the collective observations (Katzer 1904; Pauliš et al. 2019; this study) that the Chříč polymetallic vein mineralization is intimately associated with the local spessartite dike, with hydrothermal veins present either directly within the dike or in its thin contact-metamorphosed zone. This steeply dipping structure represents a distinct structural inhomogeneity within the rather homogeneous sequence of TBU graywackes, siltstones and volcanic rocks. As such, it likely served as a pathway for the ascent of hydrothermal fluids. Furthermore, textural observations are indicative for repeated tectonic activation, which resulted in ore brecciation and an ascent of hydrothermal fluids in multiple pulses, forming five stages of ore-barren or ore-bearing hydrothermal minerals.

The relationship of the studied stibnite–polymetallic mineralization to gold occurrences in the area remains to be uncertain. Three types of gold particles were recovered from the heavy concentrate from the Chříč Stream (this study), confirming previous finds indicating an overall presence of Au in the studied area. These might be, however, connected with different primary sources. For example, Malec and Novák (1982) interpreted the two abraded gold particle types as relics inherited from denuded Carboniferous sediments present in the area and the third type as being of local origin. They also found gold intergrown with quartz in one case. Our new analyses document Au contents in arsenopyrite-bearing ore (max. 0.6 ppm Au) as well as in arsenopyrite (max. 173 ppm) and pyrite (max. 33 ppm Au), collectively suggesting that some Au enrichment can be related to the initial stage of spessartite alteration and carbonate–arsenopyrite precipitation (Stage I).

5.2. Temporal evolution of hydrothermal processes

The dated arsenopyrite is present in one generation only (see above), and despite the age uncertainties associated with the Re–Os dating of arsenopyrite fractions, the results clearly argue for a Cadomian or late Cadomian age of Stage I mineralization. One possible cause of the observed large age error is the variable admixture of pyrite. Pyrite originated either from the surrounding, predominantly Neoproterozoic TBU sedimentary successions, as indicated by the presence of TBU black shale fragments in the spessartite dike, or from the vein fill. This assumption is supported by variable single sample Re–Os model ages (Tab. 2) where the samples with no or low pyrite admixture yielded values in the range of 542–494 Ma, while sample CH33 with the highest pyrite admixture yielded single mineral model ages of 567–546 Ma. If sample CH33 is omitted from the age regression on this basis, remaining analyses combined still do not form a plausible age but still define two groups having ages of 547 ± 19 Ma (2 samples and 3 analyses) and 489 ± 24 Ma (2 samples comprising 3 analyses).

The older obtained Re–Os age interval overlaps with the maximum depositional ages of the hosting late Neoproterozoic to early Cambrian TBU sequence (Belt 2) derived from zircon U–Pb geochronology (~584–527 Ma; Žák et al. 2020). Considering the associated errors and the fact that the spessartite intrusion clearly postdates the volcanosedimentary sequence formation and that

Tab. 5 Sulfur isotope data for separated sulfide fractions

Sample No.	Mineral	$\delta^{34}S$ (‰ vs. CDT)
Ch-1 A	pyrite	–7.0
Ch-2	pyrite	–16.9
Ch-3	pyrite	–8.9
Ch-5	pyrite	–14.6
Ch-6	pyrite	–16.6
Ch-8	pyrite	–17.3
Ch-11	pyrite	–5.4
Ch-12	pyrite	–3.4
Ch-13	pyrite	–5.9
Ch-17	pyrite	–4.6
Ch-18	pyrite	–9.9
Ch-21	pyrite	–5.0
Ch-23	pyrite	–4.8
Ch-28	pyrite	–8.3
Ch-32	pyrite	–6.9
Ch-33	pyrite	–7.3
Ch-35	pyrite	–17.7
Ch-37	pyrite	–17.2
Ch-38	pyrite	–10.0
Ch-39	pyrite	–5.7
Ch-40	pyrite	–5.1
Ch-41	pyrite	–5.4
CH-15	arsenopyrite	–3.7
CH-25	arsenopyrite	–3.2
CH-27	arsenopyrite	–4.0
CH-31	arsenopyrite	–3.2
CH-33	arsenopyrite	–3.4
CH-9	boulangerite	–12.4
CH-10	boulangerite	–14.7
CH-1A	stibnite	–10.8
CH-1B	stibnite	–11.5
CH-3	stibnite	–14.1
CH-7	stibnite	–9.5
P 799	stibnite	–6.1
CH-16	galena	–6.5
CH-10	galena	–8.9
CH-22	galena	–9.0
CH-12 Sf	sphalerite	–8.7
CH-16 Sf	sphalerite	–8.1
CH-17 Sf	sphalerite	–4.8

arsenopyrite precipitation postdates the emplacement of the spessartite dike, it appears that the dike emplacement and Stage I of hydrothermal mineralization might represent closely related events in terms of the obtained age resolution. However, such interpretation is inconsistent with the predominantly compressive regime and strongly accretionary behavior of the Blovice accretionary complex at that time as well as the absence of any magmatic activity as yet documented for this time period except for the emplacement of boninite dikes in the far rear of the wedge (Hajná et al. 2018). In this respect, it is important to note that three arsenopyrite fractions from Chříč define the age of 488 ± 23 Ma (Fig. 4). Such age would be in a good agreement with the largely tensional regime of the study area and the widespread late Cambrian magmatic activity documented by the northwesterly lying Tis granite (~505 Ma; Venera et al. 2000) and southeasterly located Křivoklát–Rokycany Volcanic Complex (499 ± 4 Ma; Drost et al. 2004). The slope age of ~488 Ma defined by three samples with lower pyrite admixture is therefore considered a more realistic one.

The difference between our new Pb isotope data and those reported for Chříč by Vaněček et al. (1985) can be caused either by Pb isotope variability of galena, or by a systematic bias induced by old measurements. In fact, the development of a general lead isotope evolution model for ore mineralizations of the Bohemian Massif was hampered by the highly variable Pb isotope evolution of individual rock types assumed to be the source of metals for hydrothermal fluids (e.g., Bielicki and Tischendorf 1991; Pašava and Amov 1993). Nevertheless, considering the already gathered information on lead isotope evolution of the various rock types of the TBU (Pašava and Amov 1993) and the galena lead isotope dataset for hydrothermal ore mineralization of the Bohemian Massif (Vaněček et al. 1985), galena-bearing Stage III of the Chříč mineralization is probably not related to the Neoproterozoic–Cambrian evolution. Irrespective of the lead isotope evolution model used, if the hydrothermal mineralization was related to Neoproterozoic/Cambrian events (i.e., only several tens My younger than the Neoproterozoic host rock sequence), the galena $^{206}Pb/^{204}Pb$ value would be lower than 18.0. Such value is, however, not observed in Chříč galena (see also Bielicki and Tischendorf 1991), having Pb isotope compositions that argue for its Variscan age. If true, the wide time gap between the most likely ~488 Ma Re–Os arsenopyrite age representing Stage I and age suggested from lead isotope data of galena from Stage III indicates that the deep-reaching structure along the spessartite dike was repeatedly activated, showing hydrothermal activity both during the late Cambrian extension (alteration of the spessartite dike probably following its emplacement and carbonate–arsenopyrite formation,) and the Variscan orogeny (stibnite and polymetallic sulfidic stage of Stages II and III, respectively).

To get additional information on the timing of magmatic processes in the surrounding areas, a composite sample of detrital zircons from fluvial sediments of the local stream immediately below the ore prospect was dated. In summary, the detrital zircon U–Pb age spectra and the probability density plots of both studied samples show a multi-modal distribution of zircon ages with rare zircons of Paleoproterozoic age and several age peaks containing statistically significant Neoproterozoic, Ediacaran/Cambrian and Carboniferous ages (Fig. 6).

The major peak at approximately 500 Ma corresponds to the nearby Tis granite and other granitic bodies in

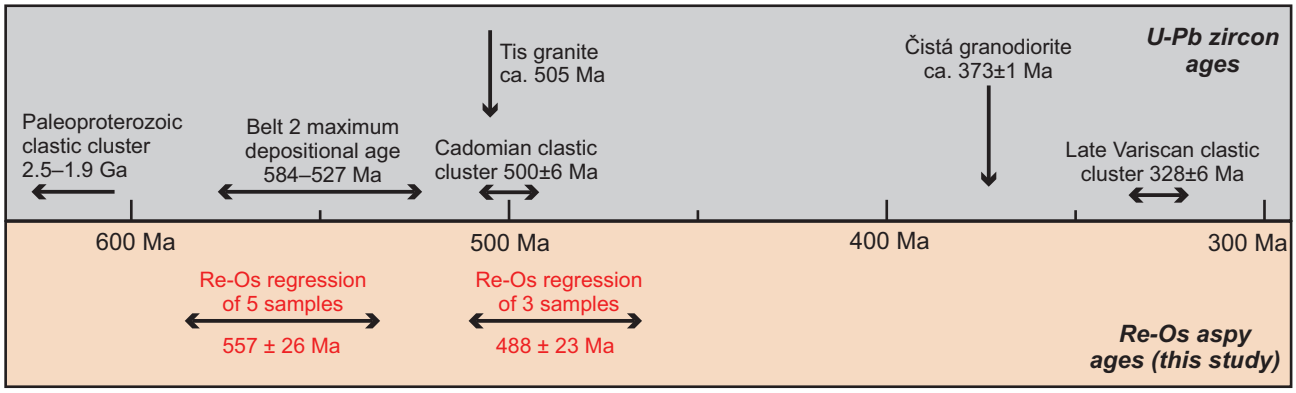

Fig. 9 Chronological relationships of the studied mineralization.

the western part of the TBU (reviewed by, e.g., Cháb et al. 2010) as well as the Křivoklát–Rokycany Volcanic Complex, collectively supporting the idea that the late Cambrian activity represents the most important magmatic pulse in the study area (Fig. 9). On the other hand, the notable absence of ~373 Ma ages in the studied zircon population, indicative of the intrusion of the Čistá granodiorite, argues against any fluvial transport of the Čistá granodiorite material into the Chříč area. A conspicuous peak of zircon age spectra at 328–330 Ma is surprising as no magmatic bodies of similar age have been reported in the adjacent part of the TBU. Two scenarios are plausible to explain this phenomenon. First, this age corresponds to certain, as yet unknown, ~330 Ma intrusions/dike rocks in the near area. Secondly, the non-abraded zircon grains indicative of a short fluvial transport were delivered to the Chříč area as a part of granitoid pebbles within Carboniferous sediments that were later locally weathered. The latter hypothesis is supported by the similarity of Chříč zircons in terms of their shape, CL characteristics, Th/U ratios and age spectra with those reported from the Carboniferous sediments (Žák et al. 2018).

5.3. Physico-chemical parameters of hydrothermal fluids and sources of ore components

In spite of the fact that fluid inclusion (FI) data could not be obtained for all mineralization stages, gathered data still provide some important insights onto physico-chemical parameters of the hydrothermal fluids. Two types of Qtz II with tight connection to sulfide mineralization were identified and confirmed by the FI study.

Both massive and breccia-type Qtz II (Stage III) contain H_2O–CO_2 fluid inclusions. Collectively, the wide range of trapping conditions together with the variable temperatures of total homogenization, temperatures of homogenization of CO_2 (thus also variable densities of the gaseous phase) argue for a fluid entrapment under widely variable temperatures from 260 to 350 °C and pressures that can be roughly estimated to range from 0.5 to 2.2 kbar (Bakker and Diamond 2000). Such characteristic mesothermal conditions of the hydrothermal fluid with a tight connection to magmatic or metamorphic activity are also supported by higher salinities of the included aqueous solution that reached up to 10 wt. % NaCl equiv.

Overall, the obtained FI temperature data clearly document that the Chříč hydrothermal mineralization is not of an epithermal type during the main ore stages. Instead, the obtained complex data indicate mesothermal hydrothermal conditions with high calculated $\delta^{18}O$ values of hydrothermal fluids (around +7.5 ‰ V-SMOW), suggesting their isotopic equilibration with hot magmatic or metamorphic rocks during their migration under crustal conditions.

Carbon isotope data argue for the crustal origin of carbon, which was largely derived from thermal decomposition of organic matter or high-temperature reaction between hydrothermal fluids and organic matter widespread in sedimentary rocks of the TBU. In addition to CO_2, both these processes also produce CH_4 detected in the studied FI by micro-Raman spectrometry. In contrast, rare limestone bodies within the sequence of the TBU (Ackerman et al. 2022 and this study) cannot serve as a source of carbon as their $\delta^{13}C$ data are distinctly different from those detected in the Chříč hydrothermal carbonates (Fig. 8). Furthermore, carbon and oxygen isotope data of hydrothermal carbonates from Chříč do not display a positive correlation between $\delta^{13}C$ and $\delta^{18}O$ values, suggesting significant changes in $\delta^{13}C$ and $\delta^{18}O$ values of fluids during the hydrothermal history.

During the mineralization stages II and III, relatively high temperatures of the hydrothermal fluids and the presence of CH_4 in the FI collectively indicate a dominance of reduced sulfur species in the hydrothermal fluids at Chříč. Under such conditions, the wide range of $\delta^{34}S$ values of sulfidic minerals (Tab. 5) can be best explained by either mixing of different sulfur sources or an involvement of a single source with highly variable $\delta^{34}S$. The

hosting volcanosedimentary units of the TBU (especially black shale horizons) are well-known for their locally elevated contents of sulfidic sulfur and extremely variable $\delta^{34}S$ values from ca. –37 to +20 ‰ V-CDT (e.g., Šmejkal et al. 1974; Hladíková et al. 1986; Hladíková and Mrázek 1988; Mrázek et al. 1990; Hladíková and Mrázek 1991; Pašava et al. 1996). Such values are indicative of highly variable local conditions of bacterial and locally also abiogenic reduction of marine sulfate during sedimentary, volcanic and diagenetic processes in the Neoproterozoic to early Cambrian. In this respect, sulfur isotope compositions of hydrothermal sulfides from Chříč with variable $\delta^{34}S$ values indicate a complex source of sulfur due to the remobilization from surrounding sedimentary successions, with a possible hypothetical participation of a deeper source in magmatic rocks.

The black shales of the TBU seem to be the most plausible source of Sb, the most characteristic metal in the Chříč ores, since Pašava (2000) reported average contents of 4 ppm and 20 ppm Sb in normal and metalliferous black shales of the TBU, respectively, with some rocks containing anomalous Sb contents of max. 183 ppm.

To conclude, the metals and sulfur at Chříč were dominantly derived from various local crustal sources, with sediments of the TBU being an important source for at least some of them.

5.4. Implications for ore metallogeny of the Bohemian Massif

The study performed at Chříč was limited by the poor availability of ore samples and the impossibility to study the hydrothermal mineralization directly in the mine. Nevertheless, available information on the site of Chříč allows a comparison with other Sb-bearing hydrothermal mineralizations in the Bohemian Massif. Particularly the Au–Sb veins of the Krásná Hora–Milešov–Příčovy ore districts located within the Central Bohemian plutonic complex of Variscan age (Němec and Zachariáš 2015, 2018; see these papers for comparison of physicochemical conditions of the hydrothermal fluids) pose a possible analog. These ore veins also follow lamprophyre dikes and strike E–W, similar to the vein at Chříč. Their mineral succession also shows some similarities, such as the early precipitation of stibnite followed by the formation of galena, sphalerite, boulangerite and carbonates (e.g., Krásná Hora). However, the major difference is the absence of abundant native gold and/or aurostibite in the Chříč mineralization.

Mineral successions and fluid types similar to those at Chříč (i.e., evolution from >300 °C H_2O–CO_2 fluids to H_2O fluids and lower mineralization temperatures) have been reported from the Variscan basement units of the Western Carpathians and Eastern Alps (reviewed by Chovan et al. 2002; Radvanec et al. 2004; see also Kiefer et al. 2020 for a new dating). These occurrences are characterized by the presence of pyrite and arsenopyrite (± fine gold) mineralization, followed by Sb (Pb, Zn) mineralization dominated by stibnite accompanied by berthierite and, finally, by Cu, Sb (±Pb, Bi, Ag) sulfides with tetrahedrite, bournonite, chalcopyrite and other sulfosalts precipitated together with quartz and carbonates. Therefore, such type of mineralization seems to be a more suitable analog for the studied mineralization at Chříč.

Chříč is a rare example of a spatially isolated, mesothermal hydrothermal mineralization located within a low-grade metamorphosed rock sequence of the TBU, spatially closely associated with a spessartite dike and its subsequent tectonic reactivations. While the early carbonatization of spessartite and arsenopyrite precipitation was presumably related with the late Cambrian evolution, the formation of its major part with stibnite followed by other sulfidic minerals seems to be triggered by the Variscan tectonothermal processes.

6. Conclusions

- Stibnite-dominated hydrothermal vein at Chříč follows a steeply dipping spessartite dike, which is emplaced in low-grade metamorphosed Neoproterozoic to early Cambrian volcanosedimentary successions of the TBU.
- Mineralogical studies identified five successive hydrothermal stages: the early stage dominated by carbonates of the dolomite-ankerite series and arsenopyrite (Stage I), quartz and stibnite stage (Stage II), carbonate stage with a wide range of sulfidic minerals (Stage III) and two post-ore stages (Stages IV–V). Gold mineralization, earlier reported from the area, is justified by the presence of gold particles in heavy mineral concentrate from the Chříč Stream as well as by elevated Au contents in arsenopyrite–pyrite.
- Re–Os dating of arsenopyrite indicates a large-scale perturbation, perhaps due to an admixture of TBU-derived pyrite and/or alteration. Yet, the data generally suggest Cadomian age of Stage I mineralization. On the other hand, Variscan age is indicated for the Stage II–III mineralizations based on galena lead isotope data.
- The fluid inclusion study argues for H_2O–CO_2-type fluids for the sulfidic ore stage III. Their high and variable Th values as well as the high $\delta^{18}O_{fluid}$ values argue for mesothermal conditions.
- Majority of carbonate carbon was derived from organic matter decomposition or organic matter reaction with hydrothermal fluid while sulfur isotope data indicate

diverse sulfur sources (e.g., remobilized TBU sulfides) or a source with a varied sulfur isotopic composition.
– The complex evolution of the Chříč ore mineralization reflects both late Cambrian (i.e., spessartite carbonatization, arsenopyrite deposition) and Variscan hydrothermal processes. The Variscan stage of the mineralization displays some similarities with Variscan stibnite veins in Slovakia and Austria, which are related to a metamorphic front development.

Acknowledgements. The study was financed by two subsequent projects of the Czech Science Foundation, GA 17-15700S and GA 20-13644S, both largely focused on the Teplá-Barrandian Unit of the Bohemian Massif. KŽ and LA also received institutional support RVO 67985831 of the Institute of Geology of the Czech Academy of Sciences. We wish to thank the authors of the paper of Pauliš et al. (2019) for a possibility to use samples from their research in our study. Information provided during the fieldwork by P. Jakubíček and J. Kounovský was highly appreciated. We are grateful to L. Polák and J. Rejšek for the collection of galena lead isotope data and Z. Lněničková, I. Jačková and B. Čejková for C–O–S stable isotope analyses, and to Roman Skála, who provided micro-Raman analyses of fluid inclusions.

References

Ackerman L, Haluzová E, Creaser RA, Pašava J, Veselovský K, Breiter K, Erban V, Drábek M (2017) Temporal evolution of mineralization events in the Bohemian Massif inferred from Re–Os geochronology of molybdenites. Miner Depos 52: 651–662

Ackerman L, Hajná J, Žák J, Erban V, Sláma J, Polák L, Kachlík V, Strnad L, Trubac J (2019) Architecture and composition of ocean floor subducted beneath northern Gondwana during Neoproterozoic to Cambrian: A palinspastic reconstruction based on Ocean Plate Stratigraphy (OPS). Gondwana Res 76: 77–97

Ackerman L, Žák K, Skála R, Rejšek J, Křížová Š, Wimpenny J, Magna T (2020) Sr–Nd–Pb isotopic systematics of Australasian tektites: Implications for the nature and composition of target materials and possible volatile loss of Pb. Geochim Cosmochim Acta 276: 135–150

Ackerman L, Žák J, Žák K, Pašava J, Kachlík V, Hora J, Veselovský F, Hajná J (2022) Carbon, oxygen, and strontium isotopic fingerprint in Neoproterozoic to early Cambrian limestones in an active margin setting: A record of local environment or global changes? Precambr Res 370: 106538

Ackerman L, Žák J, Kachlík V, Pašava J, Žák K, Pack A, Veselovský F, Strnad L (2023): The significance of cherts as markers of Ocean Plate Stratigraphy and paleoenvironmental conditions: New insight from the Neoproterozoic–Cambrian Blovice accretionary wedge. Geosci Front 14: 101478

Bakker R, Diamond LW (2000) Determination of the composition and molar volume of H_2O–CO_2 fluid inclusions by microthermometry. Geochim Cosmochim Acta 64: 1753–1764

Beaudoin G, Leach DL, Hofstra A, Seifert T, Zák K (1999) Silver–lead–zinc veins: A descriptive model. In: Stanley CJ et al. (eds) Mineral Deposits: Processes to Processing, Volume 2. A.A. Balkema, Rotterdam, pp 923–926

Bernard JH (1991) Empirical types of ore mineralizations in the Bohemian Massif. Czech Geological Survey, Prague, pp 1–181

Bernard JH, Žák K (1992) Stable isotope study of Variscan vein Pb–Zn–Ag mineralization of the Bohemian Massif. Explor Min Geol 1: 81–84

Bielicki K-H, Tischendorf G (1991) Lead isotope and Pb-Pb model age determinations of ores from Central Europe and their metallogenetic interpretation. Contrib Mineral Petrol 106: 440–461

Birck JL, Roy Barman M, Capmas F (1997) Re-Os isotopic measurements at the femtomole level in natural samples. Geostand Newslett 20: 19–27

Blažek J, Tyráček J, Mašek J, Hradecký P (1996) Geological map of the Czech Republic 1 : 50 000, sheet 12-13 Jesenice, Czech Geological Survey, Prague (in Czech)

Bodnar RJ, Vityk MO (1994) Interpretation of the microthermometric data for H_2O–NaCl fluid inclusions. In: De Vivo B, Frezzotti ML (eds) Fluid inclusions in minerals: Methods and applications. Virginia Polytechnic Institute, Blacksburg, pp 117–130

Čepek L, ed. (1961) Geological map of the Czechoslovak Socialistic Republic 1 : 200 000, sheet M-33-XX Plzeň, Ústřední ústav geologický, Praha (in Czech)

Cháb J, Pelc Z (1968) Lithology of Upper Proterozoic in the NW limb of the Barrandian area. Krystalinikum 6: 141–176

Cháb J, Breiter K, Fatka O, Hladil J, Kalvoda J, Šimůnek Z, Štorch P, Vašíček Z, Zajíc J, Zapletal J (2010) Outline of the Geology of the Bohemian Massif: the Basement Rocks and their Carboniferous and Permian Cover. Czech Geological Survey, Prague, pp 1–295

Chovan M, Schroll E, Andráš P, Ebner F, Kotulová J, Mali H, Prochaska W (2002) Stibnite mineralization of Western Carpathians and Eastern Alps: Geological, mineralogical and geochemical features. Geol Carpath 53, special issue, Proceedings of the XVII. Congres of Carpathian-Balkan Geological Association, Bratislava, September 1–4, 2002, CD, pp 1–7

Cohen AS, Waters FG (1996) Separation of osmium from geological materials by solvent extraction for analysis by

thermal ionization mass spectrometry. Anal Chim Acta 332: 269–275

Deiller P, Štípská P, Ulrich M, Schulmann K, Collett S, Peřestý V, Hacker B, Kylander-Clark A, Whitechurch H, Lexa O, Pelt E, Míková J (2021) Eclogite subduction wedge intruded by arc-type magma: The earliest record of Variscan arc in the Bohemian Massif. Gondwana Res 99: 220–246

Dobeš P, Žák K, Viets J, Leach D (1995) Epithermal Pb-Zn vein mineralization of the Stříbro ore district, Bohemian Massif, Czech Republic: Fluid inclusion and stable isotope study. In: Pašava J, Kříbek B, Žák K (eds) Mineral deposits: from their origin to their environmental impacts, Proceedings of Third Biennial SGA Meeting. Balkema. Rotterdam, pp 345–348

Dobeš P, Viets J, Žák K, Leach D (1997) Pb–Zn vein mineralization of the Stříbro ore district, Bohemian Massif: An example of epithermal fluid circulation. ECROFI XIV Meeting, Nancy. Abstracts, pp 88–89

Drost K, Linnemann U, McNaughton N, Fatka O, Kraft P, Gehmlich M, Tonk Ch, Marek J (2004) New data on the Neoproterozoic–Cambrian geotectonic setting of the Teplá–Barrandian volcano-sedimentary successions: geochemistry, U–Pb zircon ages, and provenance (Bohemian Massif, Czech Republic). Int J Earth Sci 93: 742–757

Drost K, Gerdes A, Jeffries T, Linnemann U, Storey C (2011) Provenance of Neoproterozoic and early Paleozoic siliciclastic rocks of the Teplá–Barrandian unit (Bohemian Massif): evidence from U–Pb detrital zircon ages. Gondwana Res 19: 213–231

Friedman I, O'Neil JR (1977) Compilation of stable isotope fractionation factors of geochemical interest. Geological Survey Professional Paper 440 KK. US Geological Survey, US Goverment Printing Office, Washington, pp 1–117

Goldstein RH, Reynolds TJ (1994) Systematics of fluid inclusions in diagenetic minerals. SEPM Short Course 31, Tulsa, pp 1–199

Golyshev SI, Padalko NL, Pechenkin SA (1981) Fractionation of stable oxygen and carbon isotopes in carbonate systems. Geochem Int 18: 85–99

Grinenko VA (1962) The preparation of sulphur dioxide for isotopic analysis. Zhurn Neorg Khim 7: 478–483 (in Russian)

Hajná J, Žák J, Kachlík V, Dörr W, Gerdes A (2013) Neoproterozoic to early Cambrian Franciscan-type mélanges in the Teplá–Barrandian unit, Bohemian Massif: evidence of modern-style accretionary processes along the Cadomian active margin of Gondwana? Precambr Res 224: 653–670

Hajná J, Žák J, Dörr W (2017) Time scales and mechanisms of growth of active margins of Gondwana: a model based on detrital zircon ages from the Neoproterozoic to Cambrian Blovice accretionary complex, Bohemian Massif. Gondwana Res 42: 63–83

Hajná J, Žák J, Dörr W, Kachlík V, Sláma J (2018) New constraints from detrital zircon ages on prolonged, multiphase transition from the Cadomian accretionary orogen to a passive margin of Gondwana. Precambr Res 317: 159–178

Hladíková J, Mrázek P (1988) Sulphur isotopic composition of sulphides from the rocks of the Bohemian Upper Proterozoic. Sbor geol Věd, ložisk Geol Mineral 28: 111–140

Hladíková J, Mrázek P (1991): The origin of sulphides and carbonates in the volcano-sedimentary complex of the West Bohemian Upper Proterozoic (Trnčí near Klatovy). Čas Mineral Geol 36: 39–49

Hladíková J, Šmejkal V, Pašava J, Breiter K (1986) Isotopes of sulphur, carbon and oxygen at selected localities of the Proterozoic of the Barrandian region. Věst Ústř Úst geol 61: 339–348

Horita J (2014) Oxygen and carbon isotope fractionation in the system dolomite–water–CO_2 to elevated temperatures. Geochim Cosmochim Acta 129: 111–124

Irmler A (1915) Oblasti antimonových rudních výskytů v Čechách. Horn hutn listy 10: 169–171 (in Czech)

Jackson SE, Pearson NJ, Griffin WL, Belousova EA (2004) The application of laser ablation-inductively coupled plasma-mass spectrometry to in situ U–Pb zircon geochronology. Chem Geol 211: 47–69

Katzer F (1904) Notizen zur Geologie von Böhmen. VI. Zur geologischen Kenntnis des Antimonitvorkommens von Křitz bei Rakonitz. Verh K-kön geol Reichsanst 12: 263–268

Kerkhof Van den A, Thiery R (2001) Carbonic inclusions. Lithos 55: 49–68

Kiefer S, Štefko M, Vojtko R, Ozdín D, Gerdes A, Creaser RA, Szczerba M, Majzlan J (2020) Geochronological constraints on the carbonate-sulfarsenide veins in Dobšiná, Slovakia: U/Pb ages of hydrothermal carbonates, Re/Os age of gersdorffite, and K/Ar ages of fuchsite. J Geosci 65: 229–247

Klomínský J, Jarchovský T, Rajpoot G (2010) Atlas of plutonic rocks and orthogneisses in the Bohemian Massif, Bohemicum. Czech Geological Survey, Prague, pp 1–100

Krmíček L, Stárková M, Vorel T (2009) Petrography of selected amphibole lamprophyres and associated intrusions in the NW part of the Barrandian Neoproterozoic (Rakovník area). Geosci Res Rep 2008: 169–174

Linnemann U, Pereira F, Jeffries TE, Drost K, Gerdes A (2008) The Cadomian orogeny and the opening of the Rheic Ocean: the diacrony of geotectonic processes constrained by LA-ICP-MS U–Pb zircon dating (Ossa-Morena and Saxo-Thuringian Zones, Iberian and Bohemian Massifs). Tectonophysics 461: 21–43

Malec J, Novák F (1982) Mineralogicko-geochemické studium těžkých minerálů pro úkol „Šlichová prospekce jz. části Českého masívu". Unpublished report, Archive ČGS-Geofond (in Czech)

McCrea JM (1950) On the isotope chemistry of carbonates and a paleotemperature scale. J Chem Phys 18: 849–857

Morávek P, Pouba Z (1987) Precambrian and Phanerozoic history of gold mineralization in the Bohemian Massif. Econ Geol 82: 2098–2114

Morelli R M, Creaser R A, Selby D, Kontak DJ, Horne R J (2005) Rhenium–Osmium arsenopyrite geochronology of Meguma Group gold deposits, Meguma Terrane, Nova Scotia, Canada: evidence for multiple gold mineralizing events. Econ Geol 100: 1229–1242

Mrázek P, Hladíková J, Žák K (1990) Distribution of sulfur isotopes and tectonic development of the Barrandian Proterozoic (Bohemian Massif). Čas Mineral Geol 35: 135–146

Němec M, Zachariáš J (2015) The Krásná Hora epizonal orogenic Sb–Au deposit, Bohemian Massif, Czech Republic. In: André-Mayer AS, Cathelineau M, Muchez PH, Pirard E, Sindern S (eds) Mineral resources in a sustainable world. Proceeding of the 13th Biennial SGA Meeting, 24–27 August 2015, Nancy, France, pp 497–500

Němec M, Zachariáš J (2018) The Krásná Hora, Milešov and Příčovy Sb–Au ore deposits, Bohemian Massif: mineralogy, fluid inclusions and stable isotope constraints on the deposit formation. Miner Depos 53: 225–244

Ohmoto H, Rye RO (1979). Isotope of sulfur and carbon. In: Barnes HL (ed.) Geochemistry of Hydrothermal deposits. John Wiley & Sons, pp 509–567

Pašava J (2000) Normal versus metal-rich black shales in the Barrandian Neoproterozoic of the Teplá–Barrandian Unit: a summary with new data. Bull Geosci 75: 229–240

Pašava J, Amov B (1993) Isotopic composition of lead in Proterozoic anoxic metasedimentary and volcanogenic rocks from the Bohemian Massif with metallogenetic implications. Chem Geol 109: 293–304

Pašava J, Hladíková J, Dobeš P (1996) Origin of Proterozoic metal-rich black shales from the Bohemian Massif, Czech Republic. Econ Geol 91: 63–79

Pašava J, Ackerman J, Žák J, Veselovský F, Creaser RA, Svojtka M, Luais B, Pour O, Šebek O, Trubač J, Vosáhlová E, Cividini D (2021) Elemental and isotopic composition of trench-slope black shales, Bohemian Massif, with implications for oceanic and atmospheric oxygenation in Early Cambrian. Paleogeogr Palaeoclimatol Palaeoecol 564: 110195

Pašava J, Ackerman L, Žák J, Svojtka M, Magna T, Pour O, Trubač J, Veselovský F (2023) Multi-stage metal enrichment and formation of gold mineralization in black shales: the role of high heat flow in a rift setting. Miner Depos https://doi.org/10.1007/s00126-023-01169-9

Pauliš P, Dolníček Z, Vrtiška L, Pour O, Žák K, Ackerman L, Veselovský F, Pašava J, Kadlec T, Malíková R (2019) Mineralogy of the stibnite deposit at Chříč near Rakovník (Czech Republic). Bull Mineral Petrol 27: 148–166

Pertold Z (1959) Contribution to the zonality of the Stříbro ore region. Bull Geol Surv Prague, 34: 336–349

Pin C, Gannoun A, Duponta A (2014): Rapid, simultaneous separation of Sr, Pb, and Nd by extraction chromatography prior to isotope ratios determination by TIMS and MC-ICP-MS. J Anal Atom Spectrom 29: 1858–1870

Poty B, Leroy J, Jachimowicz L (1976) Un nouvel appareil pour la mesure des temperatures sous le microscope: L'installation de microthermometrie Chaixmeca. Bull Soc Fran Minéral Cristall 99:182–186

Radvanec M, Grecula P, Žák K (2004) Siderite mineralization of the Gemericum superunit (Western Carpathians, Slovakia): review and a revised genetic model. Ore Geol Rev 24: 267–298

Reich M, Kesler SE, Utsunomiya S, Palenik CS, Chryssoulis SL, Ewing RC (2005) Solubility of gold in arsenian pyrite. Geochim Cosmochim Acta 69: 2781–2796

Rožmberský P (2010) Zaniklý chemický průmysl na Chříčsku I, II, III, IV. Vlastivědný sborník, čtvrtletník pro regionální dějiny severního Plzeňska, XX (1): 18–23, XX (2): 14–22, XX (3): 18–22, XX (4): 12–18 (in Czech)

Sedlák J (1998) Gravimetric map of the Czech Republic 1 : 500 000. Geofyzika, a.s., Prague, available at http://micka.geology.cz/en/record/basic/79586f00-6f00-1958-b017-52caa6446ca8#

Shirey SB, Walker RJ (1995) Carius tube digestion for low blank Re–Os analysis. Anal Chem 67: 2136–2141

Sláma J, Košler J, Condon DJ, Crowley JL, Gerdes A, Hanchar JM, Horstwood MSA, Morris GA, Nasdala L, Norberg N, Schaltegger U, Schoene B, Tubrett MN, Whitehouse MJ (2008a) Plešovice zircon: A new natural reference material for U–Pb and Hf isotopic microanalysis. Chem Geol 249: 1–35

Sláma J, Dunkley DJ, Kachlík V, Kusiak MA (2008b) Transition from island-arc to passive setting on the continental margin of Gondwana: U–Pb zircon dating of Neoproterozoic metaconglomerates from the SE margin of the Teplá–Barrandian Unit, Bohemian Massif. Tectonophysics 461: 44–59

Šmejkal V, Haur A, Hladíková J, Vavřín I (1974) Isotopic composition of sulphur of some sedimentary and endogenous sulphides in the Bohemian Massif. Čas Mineral Geol 19: 225–237

Vaněček M, Patočka F, Pošmourný K, Rajlich P (1985) The use of the isotopic composition of ore lead in metallogenic analysis of the Bohemian Massif. Rozpr ČSAV, Ř Mat Přír Věd 95: 1–114

Venera Z, Schulmann K, Kröner A (2000) Intrusion within a transtensional tectonic domain: the Čistá grano-

diorite (Bohemian Massif) – structure and rheological modelling. J Struct Geol 22: 1437–1454

Vermeesch P (2018) IsoplotR: A free and open toolbox for geochronology. Geosci Front 9: 1479–1493

Vorel T, Adamová M, Dušek K, Holásek O, Hradecký P, Hrazdíra P, Klečák J, Krmíček L, Krupička J, Lysenko V, Mašek D, Müller P, Skácelová D., Skácelová Z, Stárková M (2012) Basic geological map of the Czech Republic 1 : 25 000, sheet 12-321 Panoší Újezd. Map sheet and Explanatory notes, Czech Geological Survey, Prague, pp 1–106 (in Czech)

Wiedenbeck M, Alle P, Corfu WL, Griffin WL, Meier M, Oberli A, von Quadt A, Roddick JC, Spiegel W (1995) Three natural zircon standards for U–Th–Pb, Lu–Hf, trace element and REE analyses. Geostand Newslett 19: 1–23

Žák J, Kratinová Z, Trubač J, Janoušek V, Sláma J, Mrlina J (2011) Structure, emplacement and tectonic setting of Late Devonian granitoid plutons in the Teplá–Barrandian Unit, Bohemian Massif. Int J Earth Sci 100: 1477–1495

Žák J, Svojtka M, Opluštil S (2018) Topographic inversion and changes in the sediment routing systems in the Variscan orogenic belt as revealed by detrital zircon and monazite U–Pb geochronology in the post-collisional continental basins. Sediment Geol 377: 63–81

Žák J, Svojtka M, Hajná J, Ackerman L (2020) Detrital zircon geochronology and processes in accretionary wedges. Earth Sci Rev 2017: 103214

Žák J, Svojtka M, Gerdjikov I, Kounov A, Vangelov DA (2022) The Balkan terranes: a missing link between the eastern and western segments of the Avalonian–Cadomian orogenic belt? Int Geol Rev 64: 2389–2415

Žák K, Dobeš P (1991) Stable isotopes and fluid inclusions in hydrothermal deposits: The Příbram ore region. Rozpr ČSAV, Ř mat přír Věd, Academia, Praha, pp 1–109 (in Czech)

Žák K, Čadek J, Dobeš P, Šmejkal V, Reichmann F, Vokurka K, Sandstat JS (1990) Vein barite mineralization of the Bohemian Massif: Sulfur, oxygen and strontium isotope and fluid inclusion characteristics and their genetic implications. Proceedings of the Symposium on Barite and Barite Deposits, Geological Survey, Prague, pp 35–49

Žák K, Dobeš P, Sztacho P (1996) Vein-type hydrothermal deposits of the Bohemian Massif: Evolution of hydrothermal fluid sources and relation to extension events in the crust. Global Tect Metallog 5: 175–178

Zimmerhakl P (1982) Distribuce zlata a zhodnocení jeho akumulací v křivoklátsko-rokycanském pásmu a přilehlém proterozoiku. MSc Thesis, Faculty of Science. Charles University, Prague, pp 1–98 (in Czech)

Zheng Y-F (1999) Oxygen isotope fractionation in carbonate and sulfate minerals. Geochem J 33: 109–126

Zoubek V, ed. (1964) Geological map of the Czechoslovak Socialistic Republic 1 : 200 000, sheet M-33-XIV Teplice – Annaberg-Buchholz, Ústřední ústav geologický, Praha (in Czech)